

THERMAL-HYDRAULIC AND NEUTRONIC
CONSIDERATIONS FOR DESIGNING
A LITHIUM-COOLED TOKAMAK BLANKET

Jiatsong Chao
Bora Mikic
Neil Todreas

PFC/RR-79-11

FUSION TECHNOLOGY PROGRAM

Massachusetts Institute of Technology
Cambridge, MA 02139

December 1978

THERMAL-HYDRAULIC AND NEUTRONIC CONSIDERATIONS FOR
DESIGNING A LITHIUM-COOLED TOKAMAK BLANKET

Jiatsong Chao

Bora Mikic

Neil Todreas

ABSTRACT

A methodology for the design of lithium cooled blankets is developed. The thermal-hydraulics, neutronics and interactions between them are extensively investigated.

In thermal hydraulics, two models illustrate the methodology used to obtain the acceptable ranges for a set of design parameters. The methodology can be used to identify the limiting constraints for a particular design.

For typical tokamaks, the header diameter is about 12 cm; coolant inlet velocity is found to be less than 0.1 m/sec in order to maintain a reasonable hoop stress in the header. For the constant \dot{Q}' model, where tubes are distributed to match the volumetric heat generation, the limiting constraints are found to be the total number of tubes and the maximum size of the headers that can fit into the blanket radially. The maximum first wall neutron loading is 7 MW/m^2 . For the constant T_{max} model, where cooling channels are placed so that the peak temperatures between the channels are equal, the limiting constraint is found to be the thermal stress in the channel wall. The first wall neutron loading is found to be 2.1 MW/m^2 .

A complete neutronic scheme is set up for the calculations of the volumetric heating rate as a function of

the distance from the first wall, the breeding ratio as a function of the amount of structural material in the blanket, and the radiation damage in terms of atom displacements and gas production rate.

Different values of the volume percent of Type-316 stainless steel are assigned in four breeding zones to represent a nonuniformly distributed structural material which satisfies various thermal-hydraulic requirements. For a 10% average volume percent stainless steel in the blanket filled with lithium, the difference in breeding ratio between having a uniform structural distribution and an exponentially decreasing distribution is 4%. The difference in breeding ratio where the value of albedo is changed from 0.0 to 0.45 is 1%. The effects on heat generation of different structural distributions and different albedos are insignificant. For values of volume percent of stainless steel in the breeding zone ranging from 5% to 15%, the breeding ratios range from 1.481 to 1.256; thus, the amount of structural material needed to cool the blanket is not limited by the breeding ratio.

The role that the radiation damage plays in the overall design methodology is described. The product of the first wall lifetime and neutron loading is limited by the radiation damage which degrades the mechanical properties of the material.

ACKNOWLEDGEMENTS

Many people contributed towards this report. We would especially like to thank Professor Sow-Hsin Chen for his suggestions, Andrew Cook and Franklin Chen for help in running ANISN, and Tom McManamy who was working on a parallel report. We also wish to express our gratitude to Graydon Yoder and Allen Levin for reviewing this report, and to Prudence Young for typing it.

The Radiation Shielding Information Center at Oak Ridge National Laboratory deserves thanks for providing necessary data free of charge. The comments and suggestions from Robert Santoro at Oak Ridge National Laboratory and Mohamed Abdou at Argonne National Laboratory are appreciated.

The work was supported in part by the U.S. Department of Energy.

TABLE OF CONTENTS

	<u>PAGE</u>
TITLE PAGE	1
ABSTRACT	2
ACKNOWLEDGEMENTS	4
TABLE OF CONTENTS	6
LIST OF FIGURES	9
LIST OF TABLES	11
NOMENCLATURE	12
 CHAPTER 1: INTRODUCTION	 15
1.1 FOREWORD	15
1.2 LITERATURE REVIEW	17
1.3 SCOPE OF THE WORK	18
1.4 OUTLINE OF THE THESIS	20
 CHAPTER 2: THERMAL-HYDRAULIC CONSIDERATIONS	 21
2.1 MAGNETOHYDRAUDYNAMIC CONSIDERATIONS	21
2.2 CONSTANT \dot{Q}' MODEL	28
2.2.1 PHYSICAL DESCRIPTION OF THE MODEL	28
2.2.2 CALCULATION - \dot{Q}' MODEL	31
2.2.3 GOVERNING RELATIONS	36
2.2.4 RESULTS	38
2.3 CONSTANT T_{MAX} MODEL	46
2.3.1 PHYSICAL DESCRIPTION	46

	<u>PAGE</u>
2.3.2 CALCULATION - T_{MAX} MODEL	48
2.3.3 RESULTS	50
2.4 DISCUSSION	54
CHAPTER 3: NEUTRONIC CALCULATIONS	57
3.1 INTRODUCTION	57
3.2 BLANKET MODELS AND CALCULATION PROCEDURES	60
3.3 RESULTS AND DISCUSSION	68
CHAPTER 4: INTERACTIONS BETWEEN THERMAL-HYDRAULIC AND NEUTRONICS	76
4.1 OVERALL DESIGN PROCEDURES	76
4.2 INTERACTIONS BETWEEN THERMAL-HYDRAULICS AND NEUTRONICS	79
4.3 FIRST WALL CONSIDERATIONS	81
CHAPTER 5: SUMMARY CONCLUSIONS AND RECOMMENDATIONS	83
5.1 SUMMARY	83
5.2 CONCLUSIONS	85
5.3 RECOMMENDATIONS	87
REFERENCES	90
APPENDIX A: CALCULATIONAL TECHNIQUE FOR MHD PRESSURE DROPS.	94
APPENDIX B: METHODS TO CALCULATE THE HOT SPOT TEMPERATURE	101
APPENDIX C: PROGRAM WINDOW	105
APPENDIX D: DERIVATION OF $U_{H,CRITICAL}$	112

	<u>PAGE</u>
APPENDIX E: PROGRAM BEERCAN	115
APPENDIX F: PROGRAM NEBULA	131

<u>FIGURE</u>		<u>PAGE</u>
18	THE COMPARISON OF HEATING RATES USING DIFFERENT GROUP STRUCTURES	70
19	THE EFFECT OF USING DIFFERENT ALBEDOES ON HEATING	71
20	BREEDING RATIOS AS FUNCTIONS OF THE AMOUNT OF STRUCTURE MATERIAL IN BREEDING ZONE FOR HELIUM, FLIBE AND LITHIUM AS COOLANTS	73
21	A SERPENTINE TUBE ARRANGEMENT	88
A1	CROSS SECTION OF A COOLANT CHANNEL WITH CONDUCTING WALL.	97
A2	A SIMPLE MODEL FOR THE RESISTANCE IN THE POOL.	98
B1	CALCULATIONAL MODELS FOR HOT SPOT TEMPERATURE.	102
E1	FLOW CHART FOLLOWED TO DETERMINE CHANNEL POSITIONS AND PEAK TEMPERATURE IN BEERCAN	117

LIST OF TABLES

<u>TABLE</u>		<u>PAGE</u>
I	COMPARISON OF THE TWO MODELS	55
II	SUMMARY OF NUCLIDE DENSITIES	65
III	26 ENERGY GROUP STRUCTURES	66
IV	BREEDING RATIOS OF VARIOUS CONFIGURATIONS	69
V	RADIATION DAMAGE RATES IN TYPE-316 STAIN- LESS STEEL AS THE FIRST WALL MATERIAL	75
A1	THE RESULTS OF THE EXAMPLES CALCULATED FOR THE VARIOUS TYPES OF PRESSURE DROPS	100
F1	INPUT INSTRUCTIONS FOR PROGRAM NEBULA	135

NOMENCLATURE

- a_i - half width of an adiabatic box in Fig. 4 (cm)
 b_i - half length of an adiabatic box in Fig. 4 (cm)
 B - magnetic field strength (tesla)
 B_{\max} - the maximum value of magnetic field strength (tesla)
 $B.R.$ - tritium breeding ratio
 C_1 - pumping power ratio
 C_p - specific heat of lithium (joule/Kg⁰C)
 D_H - header diameter (cm)
 D_t - tube diameter (cm)
 $D_{H, i}$ - the width of the header-channel intersection area at channel i
 F_c - a safety factor in the calculation of MHD pressure drop
 H - Hartmann number
 K - thermal conductivity of lithium (joule/m-sec⁰C)
 L - major circumference of a toroidal reactor (m)
 M - energy multiplication factor - energy generated in the blanket divided by the energy of neutrons pass through the first wall
 N - number of sectors, each sector has one inlet header and one outlet header
 N_{CH} - number of coolant channels
 n - number of tubes per sector
 N_u - Nusselt number
 N_t - the total number of tubes in the blanket
 ΔP_t - total pressure drop (MPa)
 q_w - first wall loading (MW/m²)
 \dot{Q} - heat received per unit length per unit time by each tube (W/m)

- \dot{Q}''' - volumetric heat generation rate (W/cm^3)
 R_i - distance between the first wall and the coolant tube or channel i (cm)
 R_w - first wall radius (cm)
 Δr_i - effective coolant channel width (cm)
 S - a constant in Eq. (1) ($(W/cm^3)/(MW/m^2)$)
 ΔT_f - film temperature drop in the coolant ($^{\circ}C$)
 ΔT_m - temperature difference between the hot spots in the lithium pool and the tubes per unit wall loading ($^{\circ}C/(MW/m^2)$)
 ΔT_c - temperature rise in the coolant ($^{\circ}C$)
 T_{in} - coolant inlet temperature ($^{\circ}C$)
 t_H - header wall thickness (cm)
 t_t - tube wall thickness (cm)
 T_{max} - maximum temperature in the lithium pool ($^{\circ}C$)
 U_H - coolant velocity at inlet (m/sec)
 U_i - coolant velocity in channel i (cm/sec)
 v - a constant in Eq. (1) (cm^{-1})
 W_i - total heat flux into channel i from walls on both sides
 X - tube or channel length (m)
 Y - distance from the first wall (cm)
 Z - blanket thickness (m)
 α - fraction of structural material in the blanket
 β_i - cross section area of adiabatic box i
 μ - viscosity of coolant (kg/m.sec)
 ρ - mass density of lithium (kg/m^3)
 σ_c - electric conductivity of lithium ($m \cdot \Omega$) $^{-1}$

- σ_h - hoop stress of tubes or headers (MPa)
- σ_r - stress limit (MPa)
- σ_t - thermal stress on tube (MPa)
- σ_w - electric conductivity of tube wall ($m \cdot \Omega$)⁻¹
- $\Delta T_{m,edge}$ - ΔT_m value at the outer edge of the blanket
- λ - lifetime of the first wall (year)

CHAPTER 1
INTRODUCTION

1.1 Foreword

Lithium, helium and flibe (LiF-BeF_2) have been considered as the primary candidates for coolants in tokamak fusion reactor blankets. Each coolant presents certain advantages and disadvantages. Liquid lithium metal seems to be the logical first choice since the blanket will need lithium to breed tritium; however, the widely recognized MHD effects encountered, when conducting fluids are moved across magnetic fields, could cause high system pressure drops.

In order to achieve acceptably low pumping power and high heat transfer coefficients, helium must be used at moderately high pressure. Helium also has a neutronic disadvantage because the relatively large ducts for coolant passages represent potentially serious neutron streaming paths; furthermore, the breeding ratios achieved by helium-cooled systems are low compared with lithium-cooled ones.

Flibe appears to offer a compromise. It has a relatively low vapor pressure at temperatures of interest and can be pumped through a magnetic field with little MHD - pressure drop. It offers better heat transfer than helium, but less breeding ratio than lithium. The most significant disadvantages are the high melting point for flibe and material compatibility problems.

The MIT fusion group⁽¹⁾ has undertaken a study to evaluate and

compare the uses of these coolants, and to ultimately offer a figure of merit, based on which the best coolant can be determined for a given fusion reactor blanket. In order to accomplish this task, a series of systematic studies, quantitatively evaluating the design constraints for different systems geometries, is required.

1.2 Literature Review

One finds in reviewing the literature on fusion blanket technologies that papers and reports published on this subject have focused on the qualitative discussion of the system's design requirements, identification of problems and difficulties, and the development of methods for future analyses^(2,3,4). Little quantitative insight has been presented. Nevertheless, several specific designs for fusion reactor systems have been proposed, including physical dimensions and other features⁽⁵⁻¹⁵⁾. However, in none of these designs have the geometry and the operating parameters been optimized to achieve the best operating condition for the coolant chosen. For example, in a lithium-cooled system, the design could be based on the pumping power limit due to high MHD pressure drops. But one can easily reduce the pumping power by using a larger duct or delivering coolant at a lower velocity. In the latter case, the temperature of the coolant could rise significantly at exit. This would cause high temperatures in the blanket near the outlet region. Temperature in the blanket would then be the design constraint. If one employs a large number of coolant channels or tubes, the temperature in the blanket could be decreased; however, the use of more tubing material may well cause a decrease in tritium breeding ratio. In order to achieve an optimal design, it may be necessary to seek a compromise among design constraints. This is true not only for the given example, but for helium- and flibe-cooled systems, as well. Thus, the information given by these specific designs is insufficient to be used to compare the coolants and determine the best of the three.

1.3 Scope of the Work

The objective and the scope of this thesis is to develop a methodology for obtaining the acceptable ranges of operating parameters (design window) for blankets cooled with lithium. A specific design can be extracted from the design window by choosing the appropriate design limits. The specific design can be used for the comparison between systems using other coolants. The parameters under consideration are the first wall neutron loading, coolant channel length, diameter of coolant tubes and headers, thickness of tubes and headers, number of tubes, number of modules, and coolant velocities.

To obtain such a design window, the principles of conservation of energy, conservation of mass, and conservation of momentum must be satisfied as well as all other thermal-hydraulic constitutive relations. The constraints to be satisfied include upper bounds on pumping power, stress level, temperature, fraction of structural material in the blanket, and number of tubes.

As part of the integrated design methodology, neutronic calculations are pursued to support the thermal-hydraulic analyses. These calculations provide tritium breeding ratios, volumetric heating rate in the blankets and radiation damages caused by high-energy neutrons. Both breeding and heating are dependent on the amount of structural material and coolant used in the breeding region. The volumetric heating in the blanket as a function of distance from the first wall is required for heat transfer analysis of the blanket design. The limit on the allowable

quantity of structural material in a blanket, to achieve an acceptable breeding ratio, brings forth an engineering design constraint. The term (λq_w) represents the product of the blanket lifetime and the first wall neutron loading. The limit on this parameter is dominated by changes of the material properties, caused by the high radiation damage rate near the first wall.

1.4 Outline of the Thesis

The work reported here is organized as follows: Chapter 2 will be concerned with thermal-hydraulics. Two design models, one based on constant \dot{Q}' , the other on constant maximum temperature, are used to arrange the cooling tubes between the headers, in order to perform the thermal-hydraulic analyses. In the constant \dot{Q}' model, tubes are spaced so that each tube will receive an equal amount of heat. In the second model, tubes are concentrated at several radial positions to form "coolant channels". The channel positions are chosen so that the maximum temperatures between the channels are the same. The detailed methodology and the comparison of these models are presented in the chapter.

In Chapter 3, a complete scheme of fusion neutronics is established using a number of codes such as TAPEMAKER and ABTR, as well as ANISN and NEBULA. Effects on breeding and heating due to the use of different albedo values and different input geometry configurations are examined. The results on \dot{Q}''' , breeding and radiation damage are produced and used to support the thermal-hydraulic calculations.

In Chapter 4, the interactions between thermal-hydraulics and neutronics regarding arrangement of cooling tubes and calculation of \dot{Q}''' are discussed. The roles that the breeding ratio and radiation damage play in the overall design methodology are described.

Finally, in Chapter 5, the results and conclusions of the study will be summarized together with recommendations for future work. Several appendices are included containing subsidiary analyses and techniques supporting the work reported in the main text.

Chapter 2

Thermalhydraulic Considerations2.1 Magnetohydrodynamic Considerations

In a fusion power system the hot fusion plasma would be in a vacuum vessel, but would be kept away from the walls by strong magnetic fields. A substantial fraction of the energy release of the fusion reactions would appear in the form of high-energy neutrons. The kinetic energy of these neutrons would be converted into thermal energy in a moderator blanket of liquid lithium which would surround the plasma just outside the inner wall. The neutrons would be slowed down by collisions with the Li nuclei, thereby transferring the neutron energy to the Li. The Li would be carried in pipes to a heat exchanger where it would deliver heat to the working fluid of an electric power plant.

The magnetic coils used to generate the high-strength magnetic fields must be outside the high neutron flux regions. As a result, they would have to be outside the Li blanket. This, in turn, means that the Li flow pipes must pass inside the magnetic field region. Since there are large pressure losses associated with the motion of conducting fluids in magnetic fields, magnetohydrodynamic (MHD) problems should be given special attention in the design of fusion reactor blanket.

To define the flow regime of Li-coolant in the blanket regions, we make use of the following dimensionless parameters:

Transverse Hartmann number,

$$H_{\perp} = |DB_{\perp} \sqrt{\frac{\sigma_c}{\mu}}|$$

parallel Hartmann number,

$$H_{||} = |DB_{||} \sqrt{\frac{\sigma_c}{\mu}}|$$

For flows without presence of a magnetic field, Reynolds number Re is sufficient to determine whether the flow in a pipe or channel will be in the laminar or turbulent flow regime. The transition Reynolds number is around 2300 for fully-developed flow in a smooth walled pipe or channel.

When a magnetic field is applied to the flow of an electrically conducting fluid, the transition Reynolds number becomes a function of the Hartmann number H because the Lorentz or $U \times B$ forces tend to suppress turbulence. This magnetic damping effect delays the transition from laminar to turbulent flow to higher Reynolds numbers. The new transition Reynolds numbers can be shown as: $Re_{\perp} = 500 H_{\perp}$, for flow parallel to B field and $H > 20$

$Re_{||} = 60 H_{||}$, for flow perpendicular to B field and $H > 40$. (16-21)

In the fusion reactor Li blankets, calculations indicate that we are almost always in the laminar flow regime due to the high Hartmann numbers encountered.

An electrically conducting channel wall in good electrical contact with the fluid can provide a return path for magnetically induced currents in the fluid resulting in a large pressure drop due to electromagnetic body forces. The steady state electromotive force is proportional

to $U \times B$, where U is the local fluid velocity and B is the magnetic strength. Therefore, in any conduction region where $(U \times B) \cdot d\ell$ is non zero, local electrical eddy currents will be induced. The phenomena responsible for MHD behavior of the fluid can be categorized in three ways:

1. If the channel walls are electrically conducting, eddy currents generated in the fluid can return through these walls, resulting in a net electromagnetic body force in the fluid which opposes its motion (Fig. 1).
2. Electrical eddy currents flow in "end regions" in a plane perpendicular to the magnetic field where the liquid enters or leaves the magnetic field or where there are gradients of magnetic field strength. These eddy currents also result in a net retarding electromagnetic body force (Fig. 2).
3. When flow turns its direction from perpendicular to parallel to B field, or vice versa, additional pressure drops are induced at pipe corners.

Without the presence of the poloidal field, the Li coolant in the parallel tubes could be in the turbulent regime. According to the Lyon-Martinelli liquid metal heat transfer correlation, for Peclet Number equal to 300 the Nusselt number is greater than 9. When a poloidal field, which is perpendicular to the tubes is assumed, the Nusselt number will approach a value of 7 as the Hartmann number gets larger than 100⁽²²⁾. In this thesis a Nusselt number of 6.9 is used. Axial heat conduction along the coolant channel is neglected.

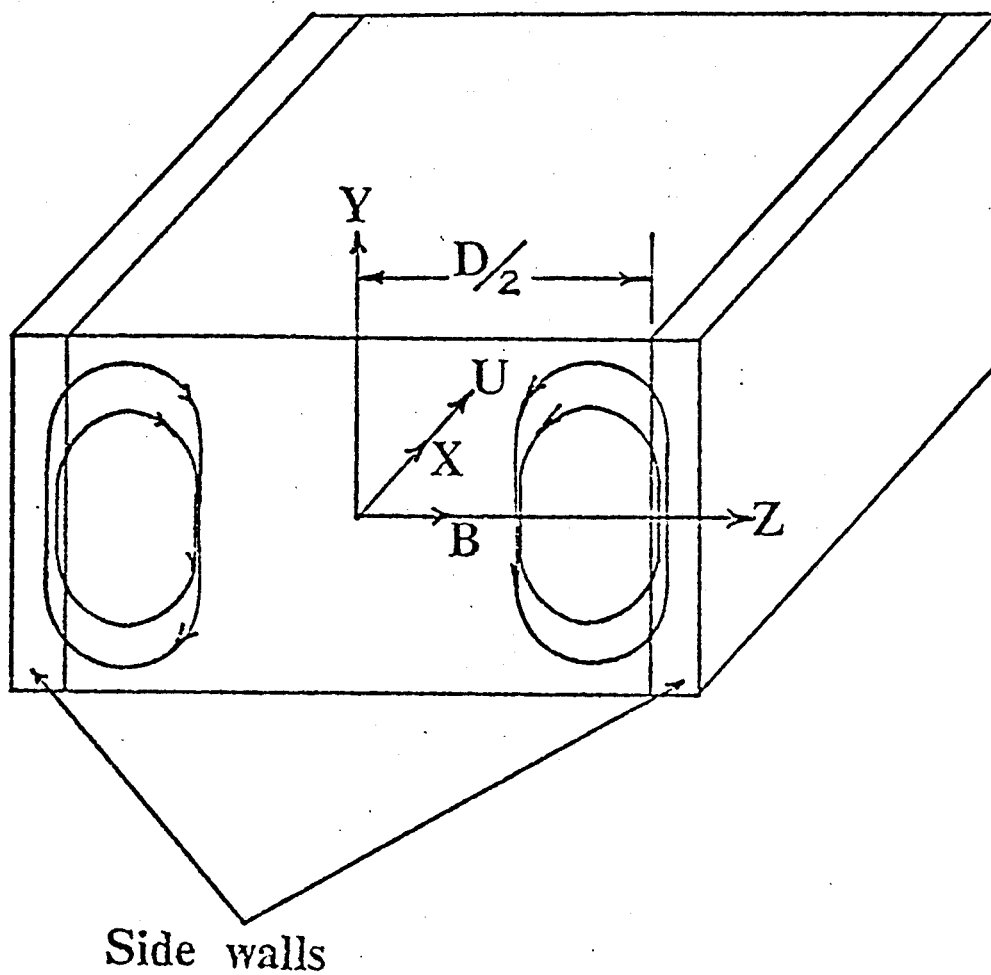


Figure 1. Effect 1 in a magnetic field B.

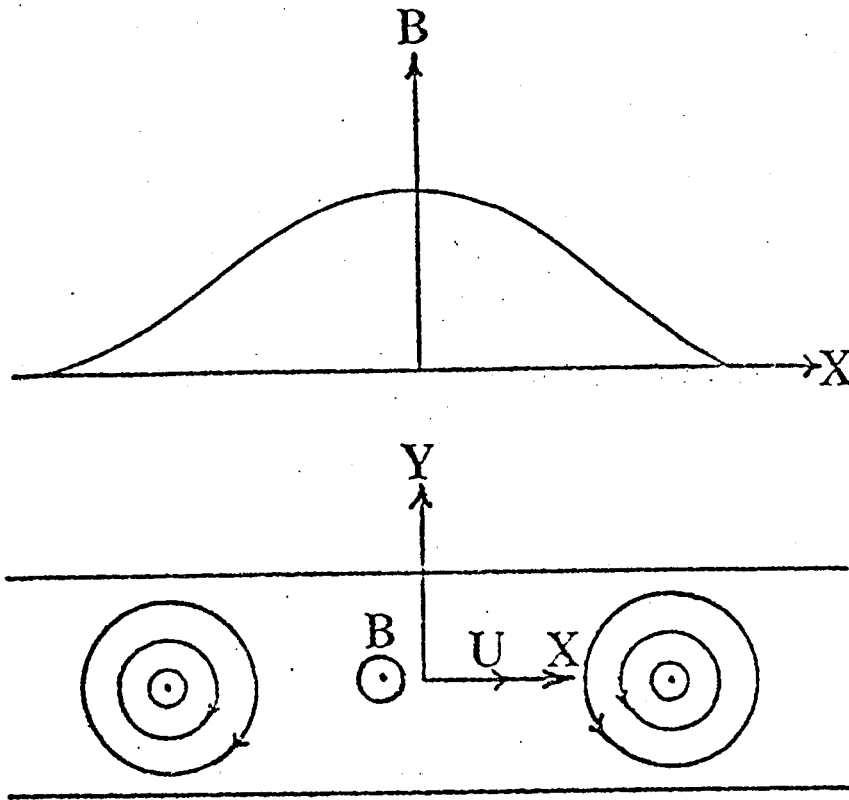


Figure 2. Effect 2 in a space-varying field.

There are four contributing terms to the total pressure loss: the MHD pressure loss in the header due to the perpendicularity of the fluid to the B field, the friction pressure loss everywhere, the MHD corner effect when the flow changes its direction at the intersection of the header and the tube, and the MHD end effect when fluid sees the magnetic field changing as it passes through the inlet or outlet regions. Compared to the MHD losses, the friction loss is insignificant. Experimental evidence indicates that the corner pressure drop will not cause as severe a problem as predicted theoretically ⁽²³⁾, and is small compared to ordinary transverse MHD duct effects. To calculate the end pressure drops, one must know the time and space distribution of the magnetic field, which varies from one specific design to another.

Hence, a safety factor is introduced to accommodate the uncertainties of existing calculation models for pressure drops. The total pressure drop is taken and is defined as the header MHD pressure drop times a safety factor. The safety factor is chosen such that the sum of pressure drops due to the space variation of magnetic field in the blanket, end effects at header entrance and exit near reactor outer edge, corner effects, friction, and MHD effect in the header, in any of the configurations used for this study, is always less than the total pressure drop. The philosophy of introducing the safety factor is to keep the methodology of the systematic analysis valid, until better models become available, by adjusting the safety factor as a parameter. Better models are needed to include effects due to time varying field and flow in a variable cross-

section pipe in a transverse or parallel field. In this study, the safety factor is conservatively taken to be 1.6. The actual sum of pressure drops due to the various effects is less than 1.6 time header MHD pressure drop, as has been calculated for several specific examples. The calculations and the techniques adopted are documented in detail in Appendix A.

2.2 Constant \dot{Q} Model

2.2.1 Physical Description of the Model

Figure 3 shows the layout of the cooling tube and header arrangements. The reactor is divided into N sectors azimuthally. Each sector contains two headers and n cooling tubes between the headers. Tubes are spaced so that each tube will receive an equal amount of heat. Besides the regions of coolant passages and the tube walls, the blanket is filled with stagnant lithium.

Since the strength of the poloidal field is usually much smaller than the toroidal field, the MHD pressure losses in the tubes are neglected. The headers are perpendicular to the toroidal magnetic field B and hence the major MHD pressure drops take place in the header.

In order to have the same velocity in each tube, one has to provide the same total resistance for each flow path. Orifices of different sizes are introduced at the intersections between the header and tubes to manipulate additional pressure drops and thus adjust the flow rate in each tube.

It is not the objective of this study to select the most suitable material for the tubes; nevertheless, stainless steel is used here because of its relatively low electrical conductivity.

When stainless steel is chosen as the tubing material, the limitation on temperature is imposed by the degradation of the material properties. A recent study showed that the temperature limit was approxi-

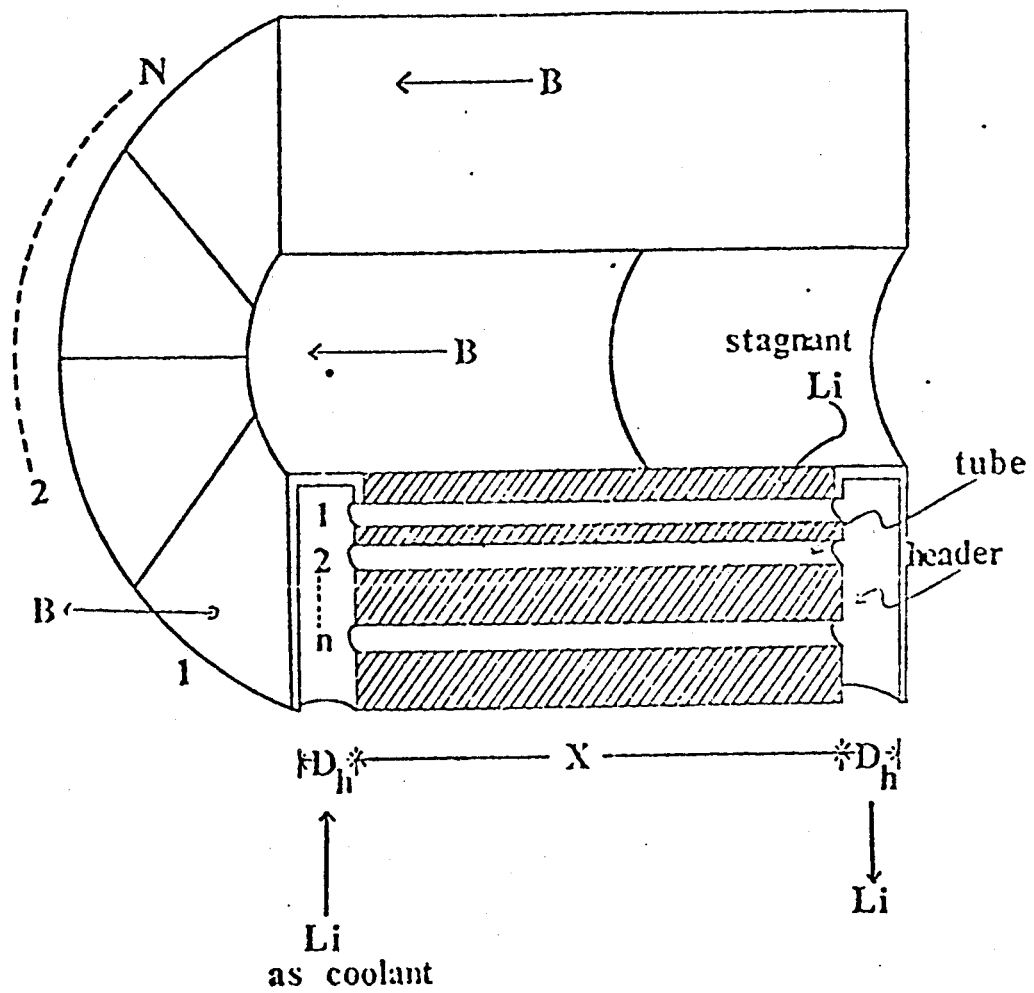


FIGURE 3. THE CONSTANT Q' MODEL

mately 500°C ⁽²⁴⁾. Thus, the temperature rise in the coolant is carefully chosen so that the wall temperature is lower than that value. Typically a lithium inlet temperature of 200°C (T_{in}) and a temperature rise in the coolant of 200°C (ΔT_c) are adopted in this study.

While the wall temperature is at low values, the peak temperatures occurring in the lithium pool between the coolant passages are inevitably high. It is possible that structural materials, used as module container walls, grids, and supporting elements between the coolant channels, could reach such high temperatures. Therefore, one must either design the structural components to be close to coolant channel to avoid high temperature, or use materials other than stainless steel, such as refractory alloys, for structural components near high temperature regions. The maximum temperature in the lithium pool is set arbitrarily from 900°C to 1000°C , simply to demonstrate the methodology of the current analysis.

2.2.2 Calculation - \dot{Q}' Model

The volumetric heat generation rate in the blanket is calculated using ANISN and NEBULA. The procedure of the calculations is discussed in the next chapter. For the thermalhydraulic analyses in this chapter, the calculated result is approximated by a curve fitted expression

$$\dot{Q}''' = S q_w e^{-vR} \quad (\text{w/cm}^3) \quad (1)$$

Since the volumetric heat generation rate decreases exponentially as the distance from the first wall increases, the distance between tubes in radial direction increases in order that each tube receives an equal amount of heat. Figure 4 is a cross-sectional view of the tube arrangement. In the model, the \dot{Q}''' is assumed constant within the adiabatic boundaries. The value of the constant, however, varies as an exponentially decreasing function of the distance from the first wall to the center of the tube.

The dimensions of the "adiabatic box" are determined by satisfying the requirement of constant \dot{Q}' , (c.f. Fig. 4) as

$$\dot{Q}' = \int_{\text{box 1}} \dot{Q}''' (R_1) d\beta_1 = \int_{\text{box 2}} \dot{Q}''' (R_2) d\beta_2 = \dots = \int_{\text{box n}} \dot{Q}''' (R_n) d\beta_n \quad (2)$$

or

$$a_1 b_1 \exp [-VR_1] = a_2 b_2 \exp [-VR_2] = \dots = a_n b_n \exp [-VR_n]$$

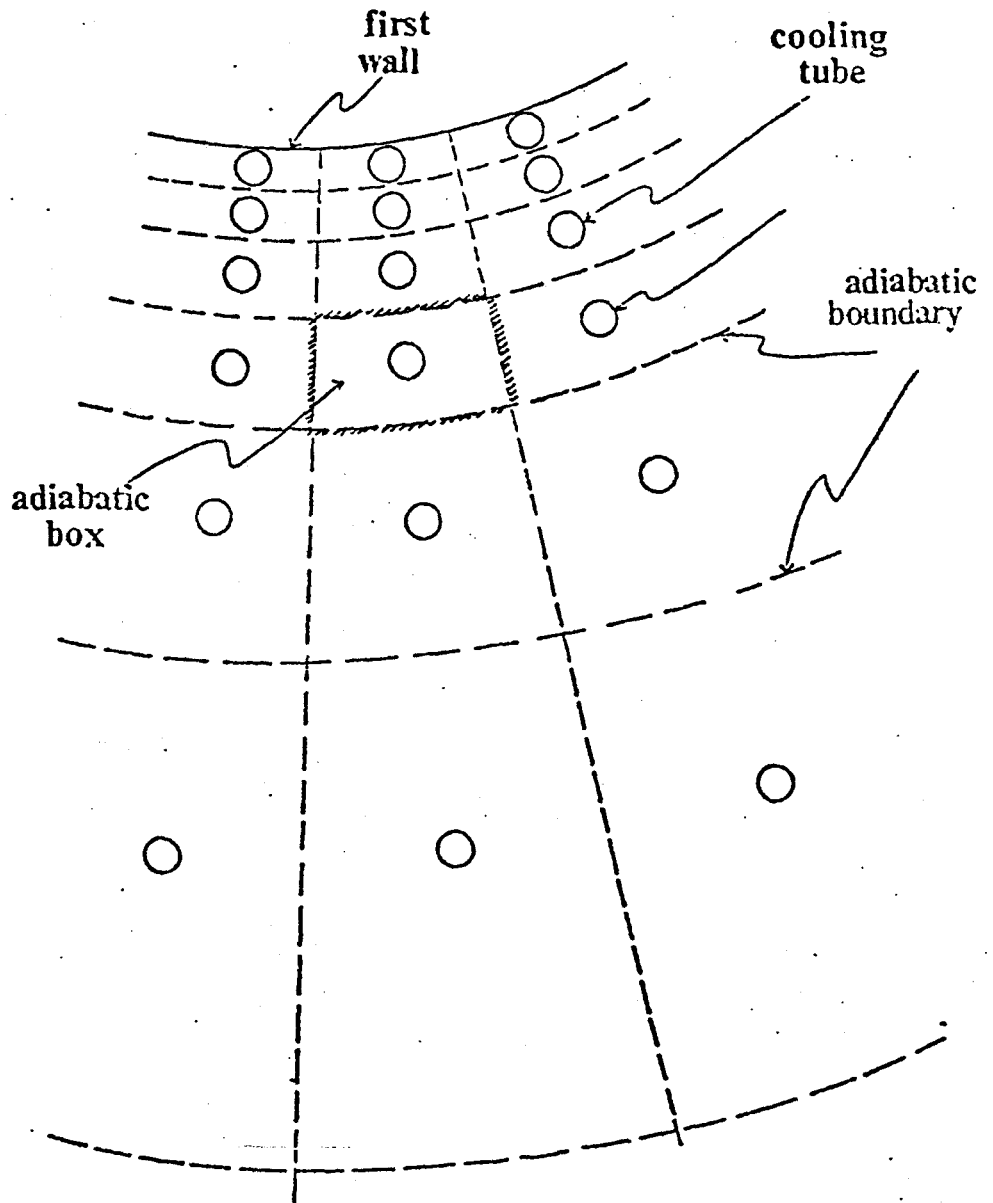


FIGURE 4. TUBE ARRANGEMENTS OF THE CONSTANT \dot{Q} MODEL (CROSS SECTION VIEW)

For geometry consideration the following expression is obtained:

$$2b_i = \frac{2\pi (R_w + R_i)}{N}, \quad i = 1, \dots, n \quad (3)$$

Therefore, a_i is found as:

$$2a_i = \frac{2 a_1 R_w \exp(VR_i)}{(R_i + R_w)}, \quad i = 1, \dots, n \quad (4)$$

where a_1 is the half width of the adiabatic box near the first wall and is taken as the tube radius if tubes are considered closely packed near the first wall. The number of tubes that can fit in the blanket radially will be:

$$n = \int_0^z \frac{dR}{2a(R)} \quad (5)$$

Thus, the relation between D_t and n is established.

The details of the methods to calculate temperature difference between the tube wall and the maximum temperature which occurs between the tubes, are shown in the Appendix B. The result is plotted in Fig. 5 for cases of $N = 78$ and $N = 117$ with $n = 13$. As can be seen from the figure, the maximum temperature in an "adiabatic box" decreases as the distance from the first wall increases, and after passing a minimum, increases again. This is because \dot{Q}''' is a rapidly decreasing function of the distance from the first wall, and thus the maximum temperature will decrease when the tube is farther from the first wall. However, to satisfy the condition of constant \dot{Q}' when \dot{Q}''' becomes small, a tube has to

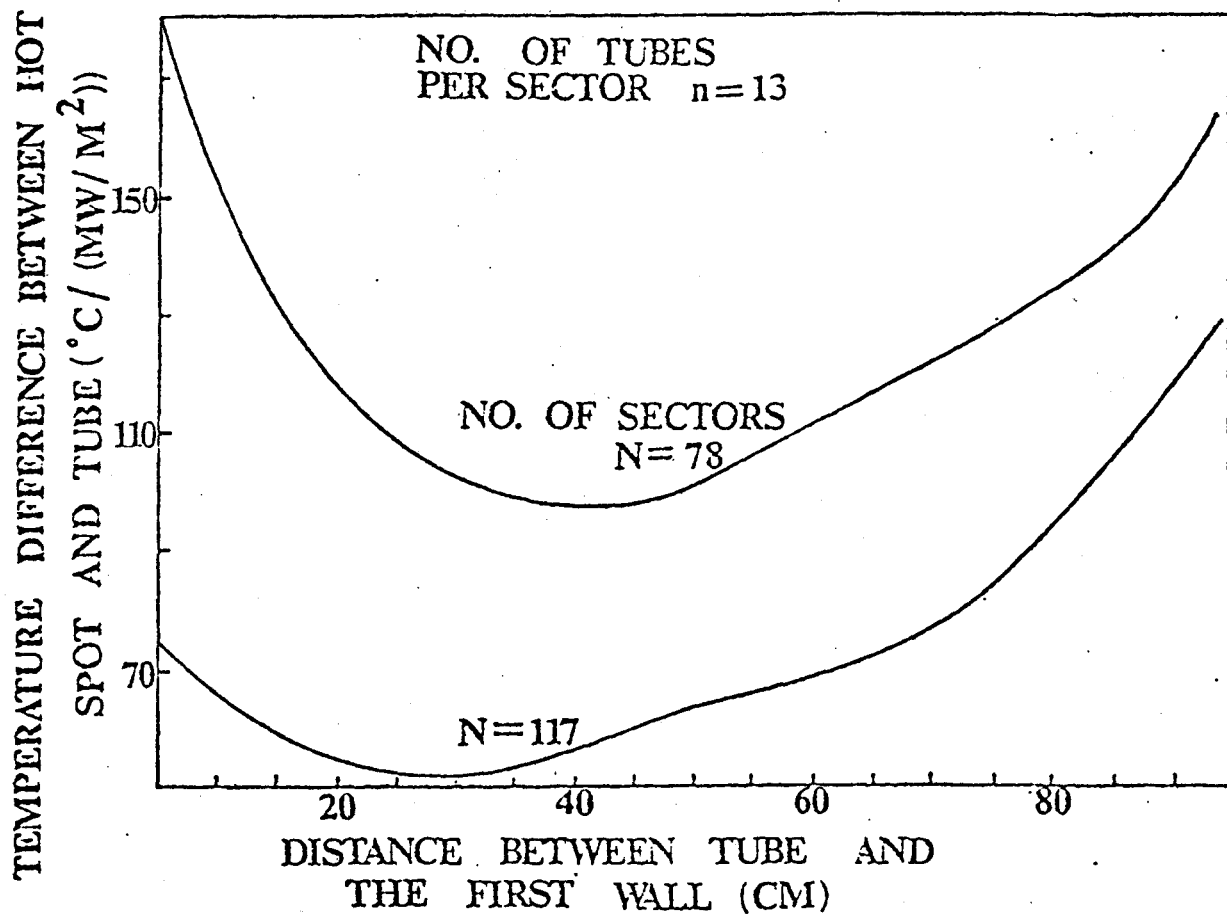


FIGURE 5. TEMPERATURE DIFFERENCE BETWEEN HOT SPOT AND TUBE IN THE BLANKET

cover a large "territory" to obtain enough heat. The longer distance, between the "hot-spot" and the tube, competes with the low \dot{Q}' and causes the ΔT_m to increase as the tube gets nearer the outer edge of the blanket.

When the blanket is divided into more sectors, i.e. N increases, one will note from the figure that the longer dimension of the "adiabatic box" near the wall and the shorter dimension of one near the outer edge of the blanket, will decrease. This explains why ΔT_m decreases more near $R=0$ region in Fig. 5, than it does near $R=Z$ region.

To avoid excessively high temperatures at the first wall, a larger value of N is chosen. A typical value of N is 160 in this study.

The following variables are taken constant through the calculation, although they may vary with temperature or position:

B_{max}	=	10	testa
K	=	38	joule/m-sec°C
ρ	=	475	kg/m ³
C_p	=	4200	joule/kg°C
S	=	4.67	(in Equation 1)
V	=	0.043	(in Equation-1)

2.2.3 Governing Relations

As discussed in the previous sections, the total pressure drop is (25)

$$\Delta P_t = 2 F_c \frac{1.3 Z B_{\max}^2 \sigma_w U_H \frac{2t_H}{D_H}}{1 + \frac{2t_H}{D_H} \frac{\sigma_w}{\sigma_c}} \quad (6)$$

The hoop stress is within a limit:

$$\frac{D_t}{2t_t} \Delta P_t = \sigma_h \leq \sigma_r \quad (7)$$

We assume that the maximum hoop stress of a tube is the same as that of a header, allowing that tubes or header might be clogged. In that case, the pressure is equalized everywhere in the passages.

Then:

$$\frac{D_H}{t_H} = \frac{D_t}{t_t} \quad (8)$$

The definition of pumping power ratio

$$\frac{N \Delta P_t (U_H \frac{\pi D_H^2}{4})^2}{\left[\int_0^Z \dot{Q}'(R) 2\pi(R+R_w) X dR \right]} = C_1 \quad (9)$$

Energy balance:

$$\left[\int_0^Z \dot{Q}'''(R) 2\pi (R+R_w) X dR \right] = N \rho U_H \frac{\pi}{4} D_H^2 C_p \Delta T_c \quad (10)$$

Heat transfer to the flowing lithium in tubes:

$$\left[\int_0^Z \dot{Q}'''(R) 2\pi (R+R_w) X dR \right] = nN N_u K X \pi \Delta T_f \quad (11)$$

The volumetric fraction of coolant tube material in the blanket:

$$\alpha = \frac{N \cdot 2 t_H \left(\frac{\pi D_H^2}{4} + Z \pi D_H \right) + N n t_t X \pi D_t}{X \pi [(R_w + Z)^2 - R_w^2]} \quad (12)$$

The total number of tubes:

$$N_t = N \cdot n \cdot \frac{L}{X} \quad (13)$$

The maximum temperature in the blanket:

$$T_{\max} = T_{\text{in}} + \Delta T_c + \Delta T_f + \Delta T_{\text{m,edge}} \quad (14)$$

The thermal stress is within a limit:

$$\sigma_t = \sigma_t(t_t, W_i, q_w) < \sigma_r \quad (15)$$

2.2.4 The Results

The analysis is carried out by the use of a digital computer. The program is documented in Appendix C. As one of the results of the analysis, the coolant inlet velocity U_H has to be less than a value $U_{H,critical}$.

When U_H is larger than $U_{H,critical}$, the increase of the header wall thickness will not reduce the hoop stress. Since an electrical conductor is used for the wall, as one can see in Fig. 6, the thicker the wall becomes the more electric current will be drawn through it, and thus causes a high MHD pressure loss. A high MHD pressure loss means high pressure is needed to deliver coolant from the inlet which will give rise to high stress in the tube wall.

When U_H is less than $U_{H,critical}$ the header (or tube) thickness can be as thin as possible and still maintain a reasonably constant hoop stress without failure, until the thickness is limited by corrosion or fabrication considerations.

The $U_{H,critical}$ is found to be:

$$U_{H,critical} = \frac{\pi}{8 F_c Z B_{max}} \sqrt{\left(\frac{C_l \rho C_p \Delta T_c}{\sigma_c} + \frac{\sigma_y}{\sigma_w} \right)} \quad (16)$$

and a typical value of $U_{H,critical}$ is 0.1 m/sec. The derivation of $U_{H,critical}$ is documented in Appendix D.

The procedure to construct the design window for the rest of the parameters of an example calculation is shown in Fig. 7 through Fig. 9.

$$t_{t2} > t_{t1}$$

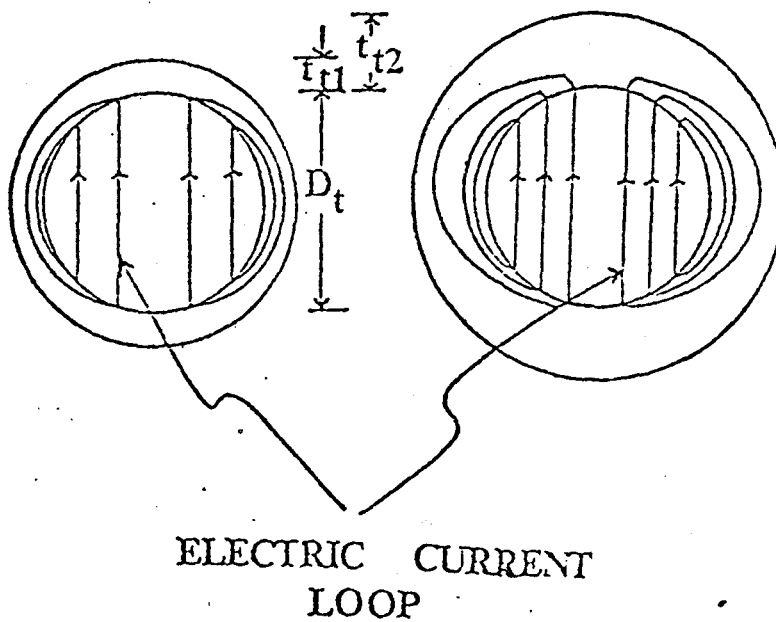


FIGURE 6. CONDUCTION WALL, ELECTRIC CURRENT
LINES CLOSE IN WALL

Figure 7 shows the relation of the total number of tubes with the tube length and the number of tubes along a header, via Equation (13).

In Fig. 8, an upper limit on the peak temperature in the lithium pool, which is likely to appear near the outer edge of the blanket in the exit region, is specified. To satisfy this limit, the first wall power must decrease as fewer tubes are employed along a header, because of the longer conduction length caused. Two horizontal lines of constant maximum first wall power in the figure can be explained by this logic.

One more variable, the temperature rise in the coolant, is held constant in Fig. 9. Unless the coolant flow rate increases, the coolant temperature will rise to a higher value after traveling in a longer tube. Since the coolant velocity is fixed at 0.1 m/sec, the header size has to be enlarged to accommodate higher flow rates, in order to satisfy the requirement of a constant temperature rise. Therefore, in Fig. 9 the diameter of the header increases in the direction of abscissa. As the number of tubes on the header increases in the direction of the ordinate, the maximum first wall power increases (as illustrated in Fig. 8). Hence, a higher flow rate is required to keep the temperature rise constant.

The result discussed and given in Fig. 7 through Fig. 9 can be combined to obtain a design window for a hypothetical reactor of given dimensions and for a given set of limiting criteria. In Fig. 10, a window is formed by the $D_H = 12.8$ cm, and $N_t = 80,000$ lines, and the x-axis. The maximum first wall load is about 6 Mw/m^2 . $D_H = 12.8$ cm is the largest header diameter at inlet for $N = 160$ and the header is tapered. Therefore,

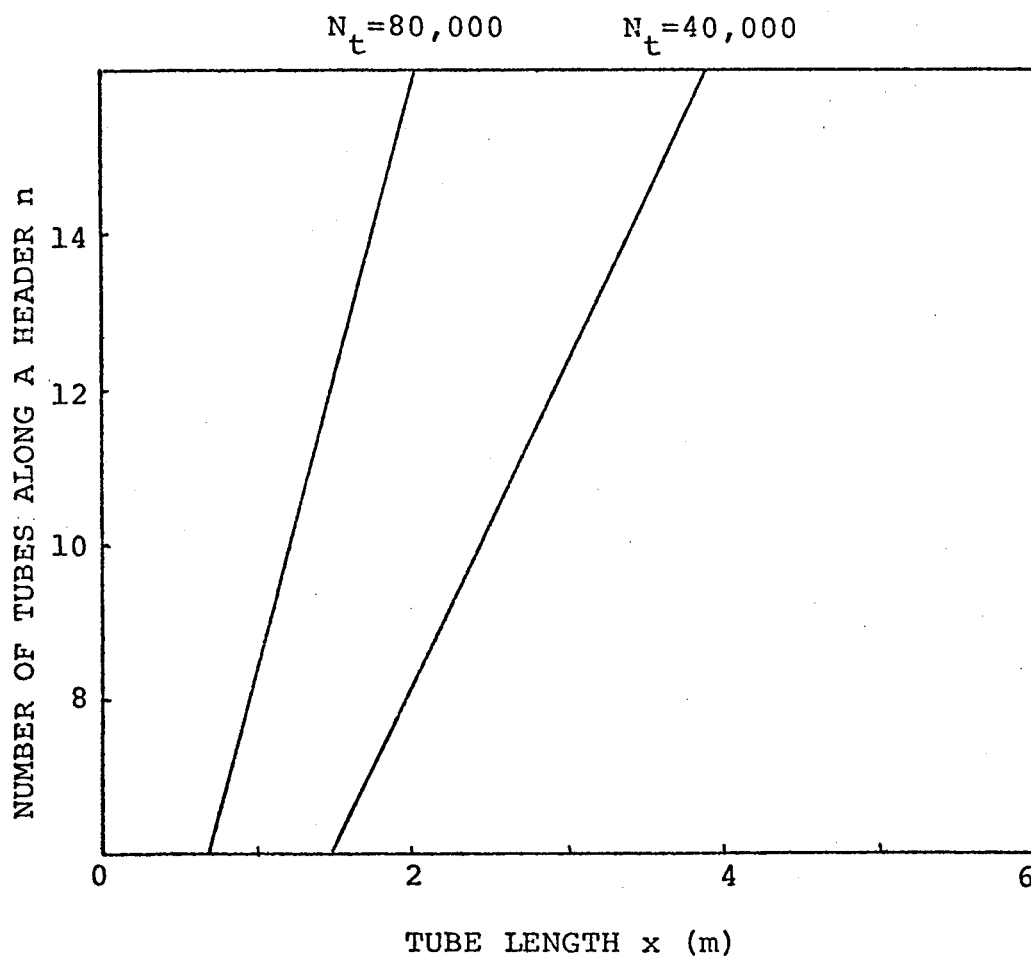


FIGURE 7. THE PLOT OF EQN. (13), $N=160$, $L=60m$.

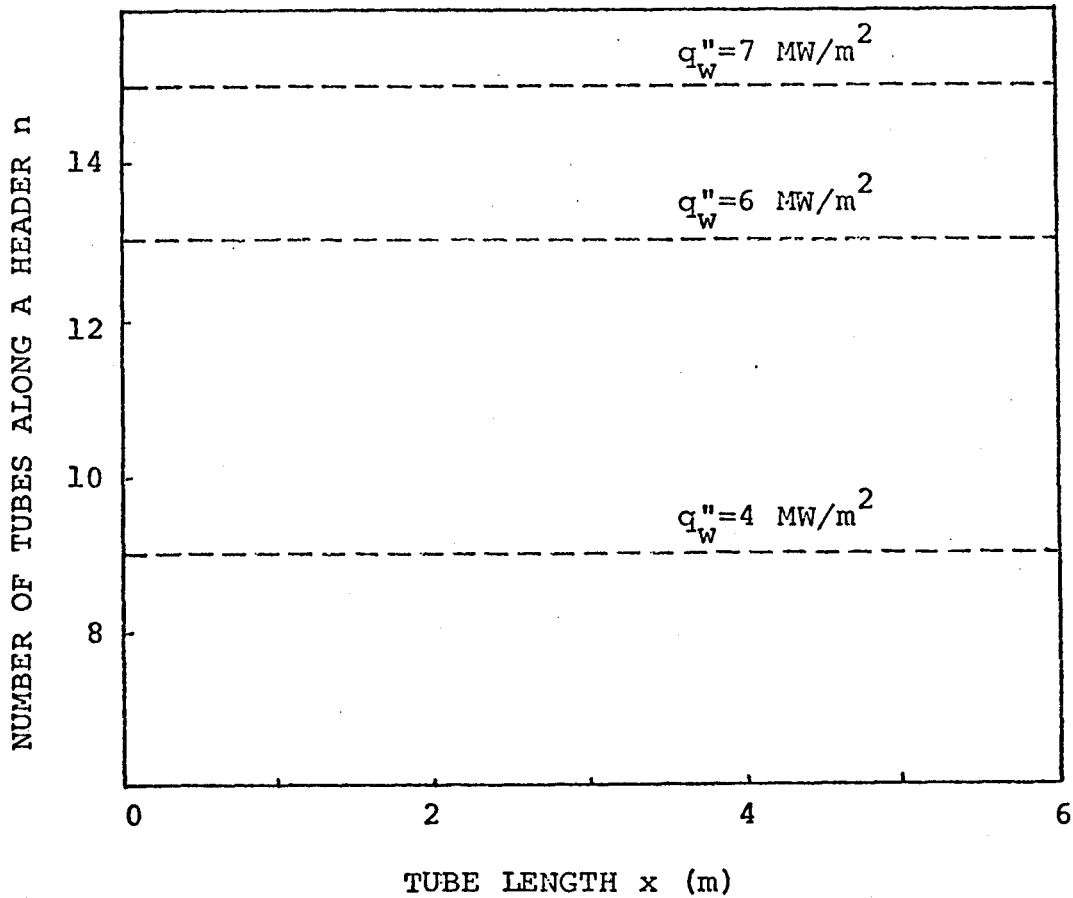


FIGURE 8. THE n - x SPACE WITH CONSTANT q_w'' LINES.

$T_{\max} = 1000^\circ\text{C}$	$U_H = 0.10 \text{ m/s}$	$C_1 = 0.010$
$T_{\text{in}} = 200^\circ\text{C}$	$N = 160$	$L = 60 \text{ m}$
$\Delta T_c = 300^\circ\text{C}$	$Z = 1 \text{ m}$	$R_w = 2.25 \text{ m}$
$t_t/D_t = t_H/D_H = 0.060$		

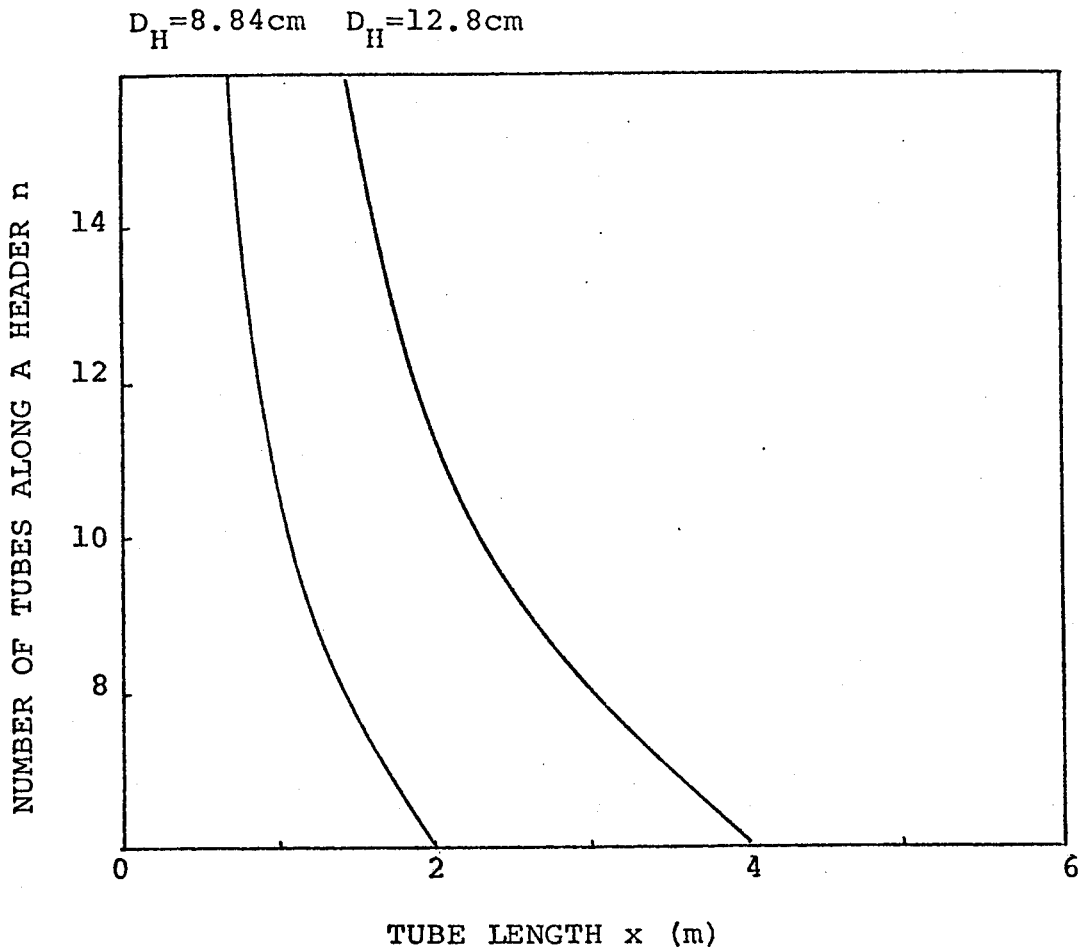


FIGURE 9. THE n - x SPACE WITH CONSTANT D_H LINES.

$T_{\max} = 1000 \text{ }^{\circ}\text{C}$	$U_H = 0.10 \text{ m/s}$	$C_1 = 0.010$
$T_{\text{in}} = 200 \text{ }^{\circ}\text{C}$	$N = 160$	$L = 60 \text{ m}$
$\Delta T_c = 300 \text{ }^{\circ}\text{C}$	$Z = 1 \text{ m}$	$R_w = 2.25 \text{ m}$
$t_t/D_t = t_H/D_H = 0.060$		

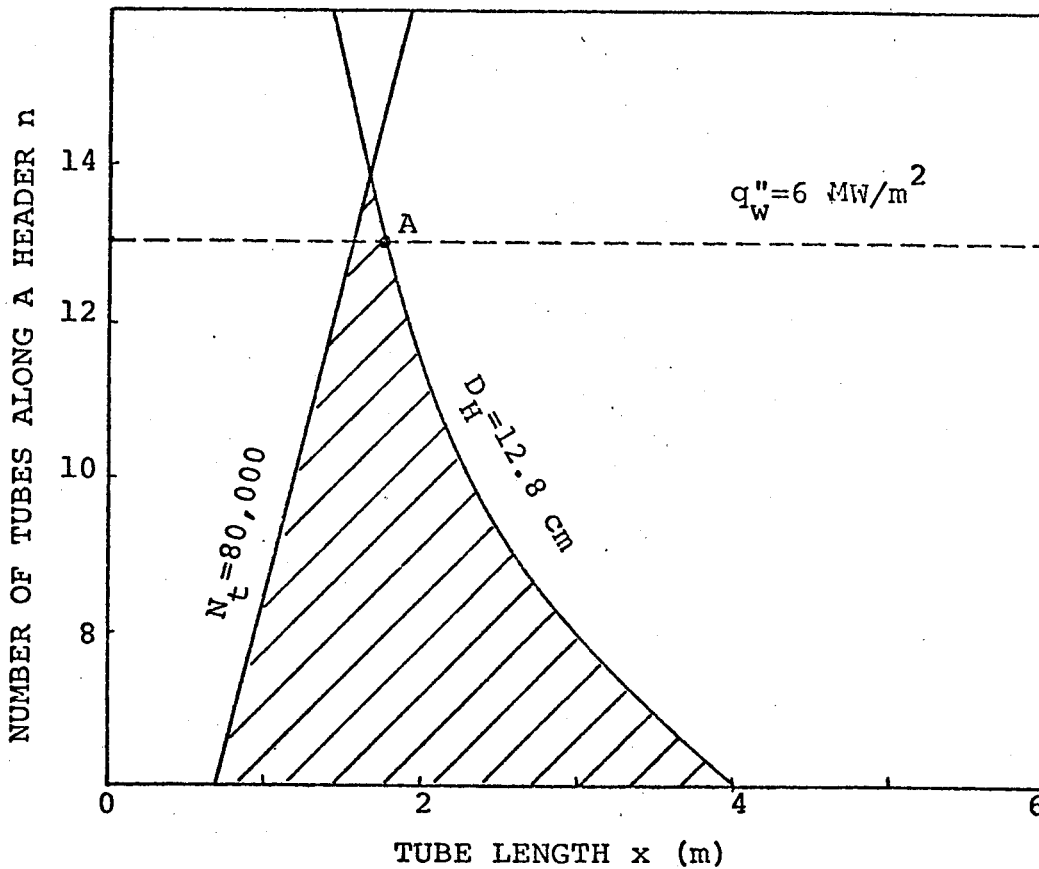


FIGURE 10. THE DESIGN WINDOW OF THE CONSTANT \dot{Q}_w MODEL.

$$T_{\max} = 1000 \text{ }^\circ\text{C}$$

$$U_H = 0.10 \text{ m/s}$$

$$C_1 = 0.010$$

$$T_{\text{in}} = 200 \text{ }^\circ\text{C}$$

$$N = 160$$

$$L = 60 \text{ m}$$

$$\Delta T_c = 300 \text{ }^\circ\text{C}$$

$$z = 1 \text{ m}$$

$$R_w = 2.25 \text{ m}$$

$$t_t/D_t = t_H/D_H = 0.060$$

the limiting constraints are the total number of tubes and the largest header size that can fit the blanket.

A thermal stress of about 20.7 Mpa is uniformly distributed in the x-n space. The value of C_1 , the pumping power ratio, is found to be below 0.01. Thus, neither the thermal stress nor the pumping power is considered the limiting design constraint in the constant \dot{Q}' model.

Taking a "design point" in the design window on the x-n plane, one can find the dimensions associated with the cooling modules. The point A in Fig. 10 gives a design with 13 tubes along a header in a module, each is 1.7 meters long and the header diameter at inlet is 12.8 cm. Such a design takes 73,000 tubes in order to operate the reactor at a maximum first wall power of 6.0 Mw/m^2 without exceeding the temperature limit of 1000°C anywhere in the blanket.

The methodology we have demonstrated here may be used in general, for different choices of structural materials, reactor dimensions or magnetic field strength, in the analysis of a hypothetical reactor.

2.3 Constant T_{\max} Model

2.3.1 Physical Description

The difference between the constant T_{\max} model and model discussed in the previous section is that the tubes, instead of spreading radially are concentrated at several radial positions to form "coolant channels" and appear as a set of concentric cylinders.

Figure 11 shows the blanket cross section of the constant T_{\max} model. The headers are tapered and are adjacent to each other. Coolant passes through the headers perpendicularly to the B field and turns into the channels, where the flow becomes parallel to the field.

The effective channel width Δr_i is assigned at channel i such that the cross sectional area of the channel is the same as that covered by tubes.

For the constant \dot{Q}' model, the design window is confined partially by the header diameter. In order to obtain a maximum coolant flow rate, an upper limit of the header diameter is assumed in the constant T_{\max} model.

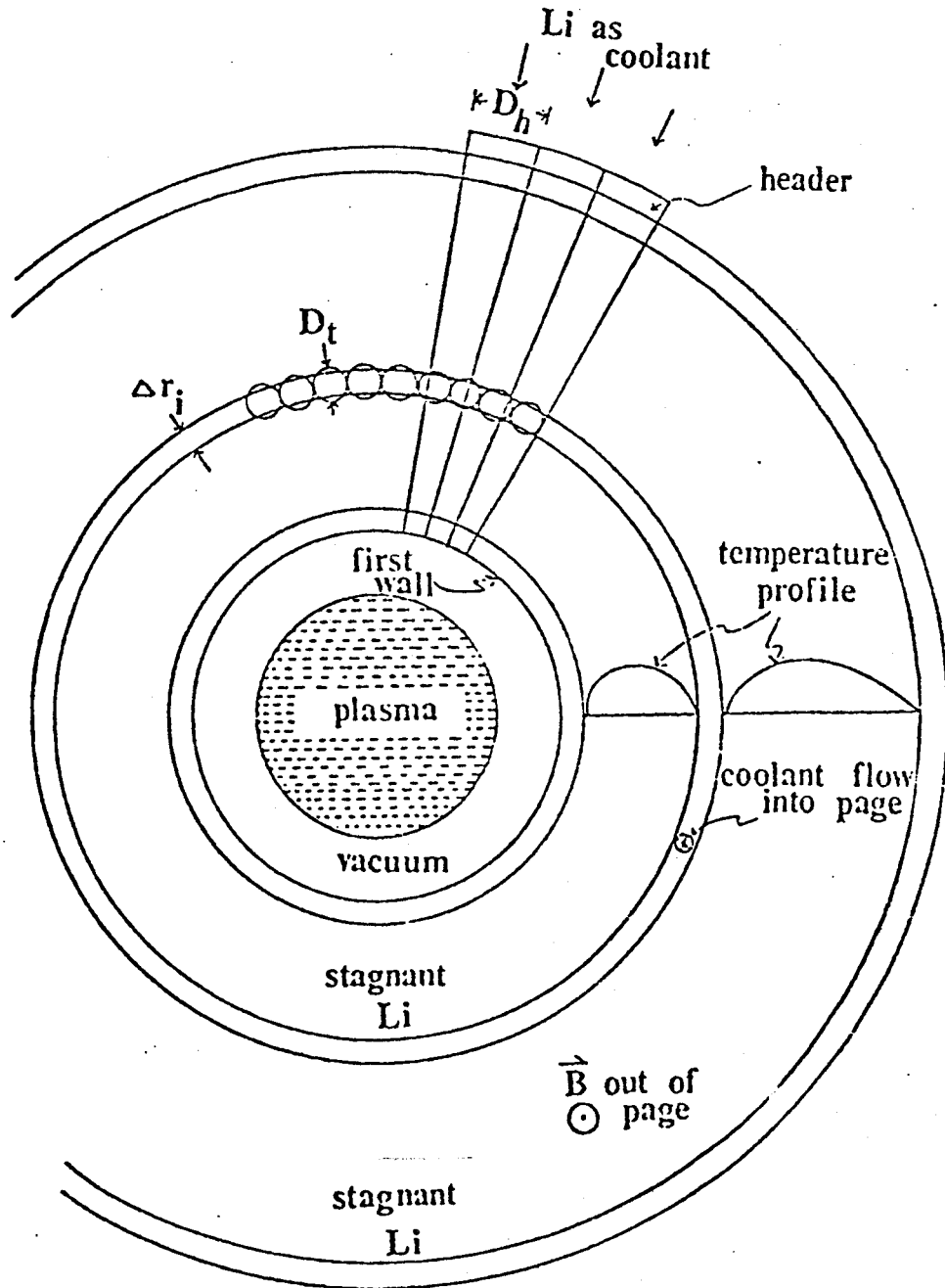


FIGURE 11. THE CONSTANT T_{MAX} MODEL

2.3.2 Calculation T_{\max} Model

All the assumptions in Section 2.2.2 remain valid. The computer code BEERCAN (see Appendix E) is developed to search for the channel positions R_i in order that in any cross sectional plane (i.e. $x = \text{constant}$ plane), the values of maximum temperature between the channels are the same, when N_{CH} and Z are given, by solving the conduction equations in cylindrical coordinates.

The boundary conditions require that the temperatures at the channel walls at equal distance from the inlet header are kept the same. Since the heat fluxes into the coolant at the walls are different from channel to channel, the coolant velocity in each channel must be adjusted by using different sizes of orifices so that the coolant temperatures rise at the same rate.

More specifically, the coolant velocities have to satisfy the following equations:

Energy balance

$$\Delta T_{c,i} D_{H,i} \Delta r_i \rho C_p U_i = X D_{h,i} W_i, \quad i = 1, \dots, N_{CH} \quad (17)$$

Continuity:

$$\sum_{i=1}^{N_{CH}} U_i D_{H,i} \Delta r_i = \frac{\pi}{4} D_H^2 U_H \quad (18)$$

With required condition:

$$\frac{\Delta T_{c,1}}{x} = \frac{\Delta T_{c,2}}{x} = \dots = \frac{\Delta T_{c, N_{CH}}}{x} \quad (19)$$

Since we have neglected conduction and natural convection in the lithium pool, the wall temperature will then increase linearly at an equal rate for all channels, with the coolant velocities solved by Eqns. (17) and (18). Hence, the temperature profile (see Fig. 11) in cross sectional plane is the same, at any distance along the channel from the header.

2.3.3 The Results

The methodology of the constant T_{\max} model is demonstrated by the analysis of a sample design using the computer code BEERCAN. The results are plotted in Fig. 12. The fixed parameters of such a design are shown at the bottom of the figure. Since the header size and the coolant velocity are kept constant, the coolant flow rate is fixed. Therefore, to achieve a constant temperature rise in the coolant, the first wall loading must be lessened as the tube length increases. The $N_{\text{CH}} - X$ space of the figure can be then visualized as an $N_{\text{CH}} - q_w$ space. As the first wall loading decreases in the direction of the abscissa at a given value of N_{CH} , the thermal stress in the channel wall decreases because a smaller amount of heat is generated in the blanket. As N_{CH} increases in the direction of the ordinate at a constant q_w or X value, the thermal stress decreases. This occurs because a smaller amount of heat is incident on a channel, due to an increase in the number of channels employed. The two thermal stress curves shown in the figure can be explained by this logic. The same reasoning applies to a set of constant T_{\max} curves. Nevertheless, only one constant T_{\max} curve ($T_{\max} = 1000^\circ \text{C}$) is shown in the figure.

It is clear that as N_{CH} increases along the ordinate, the value of the fraction of structural material in the blanket (α) becomes larger. However, at a given value of N_{CH} , decreasing X also causes an increase in α . This occurs because the adoption

of a shorter tube length causes an increase in the number of modules required to cool the whole reactor; hence, more headers are needed, which will cause α to increase.

The two constant N_t curves are obtained using the same method as the N_t lines in Fig. 7.

In Fig. 13, the design window is obtained by choosing the following design limits: $\sigma_t = 41.4\text{Mpa}$, $N_t = 80,000$ and $\alpha = 4\%$.

For example, design point A (in Fig. 12) gives the channel axial (in X direction) length 4.5 meters, when four coolant channels are used in the blanket. Such a system can operate up to a first wall load of 1.8 Mw/m^2 .

Although the result of a specific design is shown, the methodology used can apply to the cases where the blanket is composed of heterogeneously distributed materials or has a different Q''' as a function of position.

To choose an appropriate value for stress limit is not the goal of this thesis. From a recent study, a stress value between 69 Mpa and 138 Mpa, for stainless steel at operating temperatures up to $\sim 600^\circ\text{C}$, was used to identify the most life-limiting mechanical properties along with other radiation effects (26). Hence, a value lower than 69 Mpa for the stress limit is arbitrarily chosen to demonstrate the methodology represented by the design window.

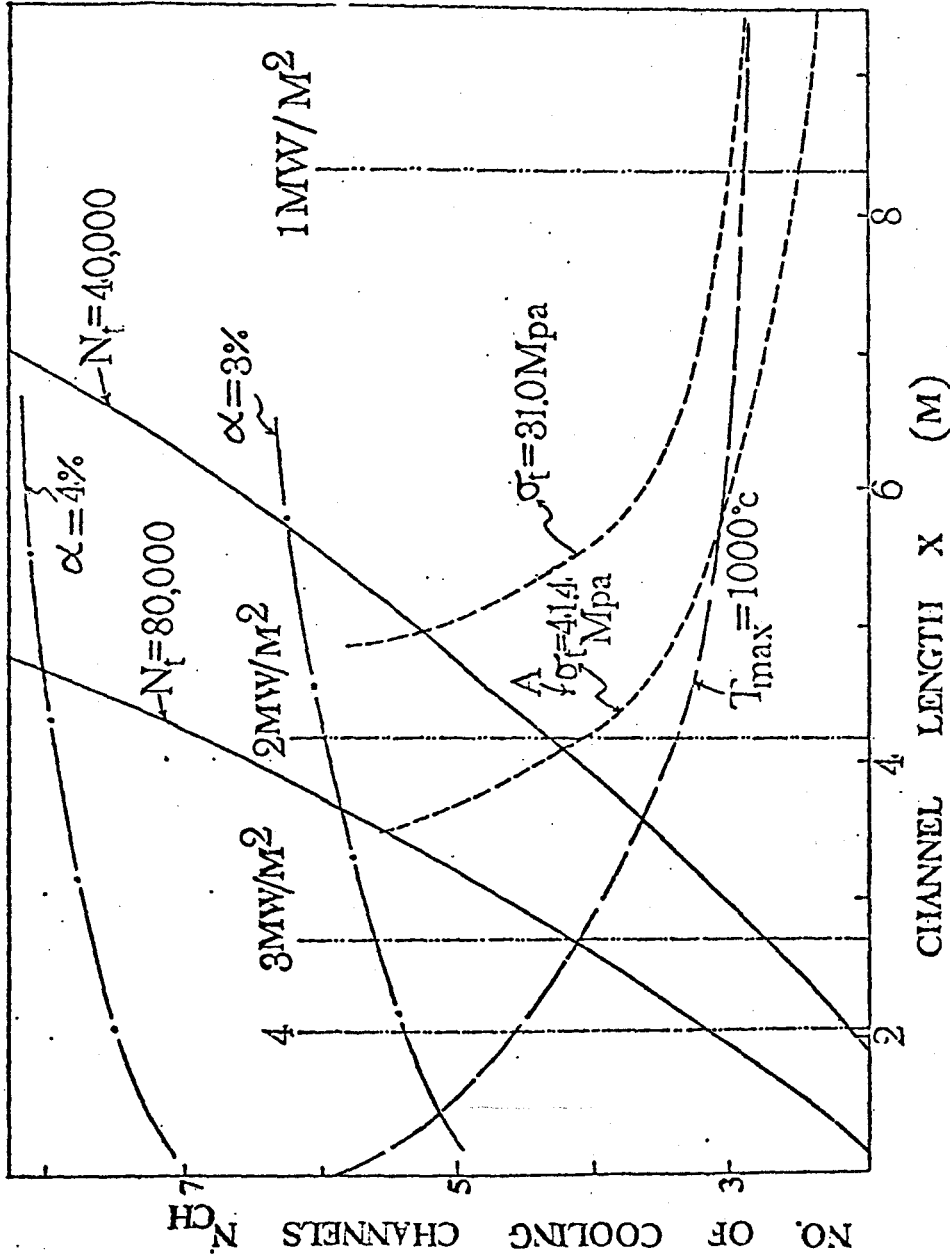


FIGURE 12. THE DESIGN WINDOW OF THE CONSTANT T_{MAX} MODEL. THE FOLLOWING PARAMETERS ARE HELD CONSTANT:

$D_{II} = 12.16$ cm $L = 60$ cm $\Delta T = 300^\circ C$ $T_{IN} = 200^\circ C$
 $Z = 1$ cm $N = 160$ $u_{II} = 0.1$ M/sec
 $r_w = 3$ m $T_{max} = 1000^\circ C$ $\Delta r_1 = 2$ cm

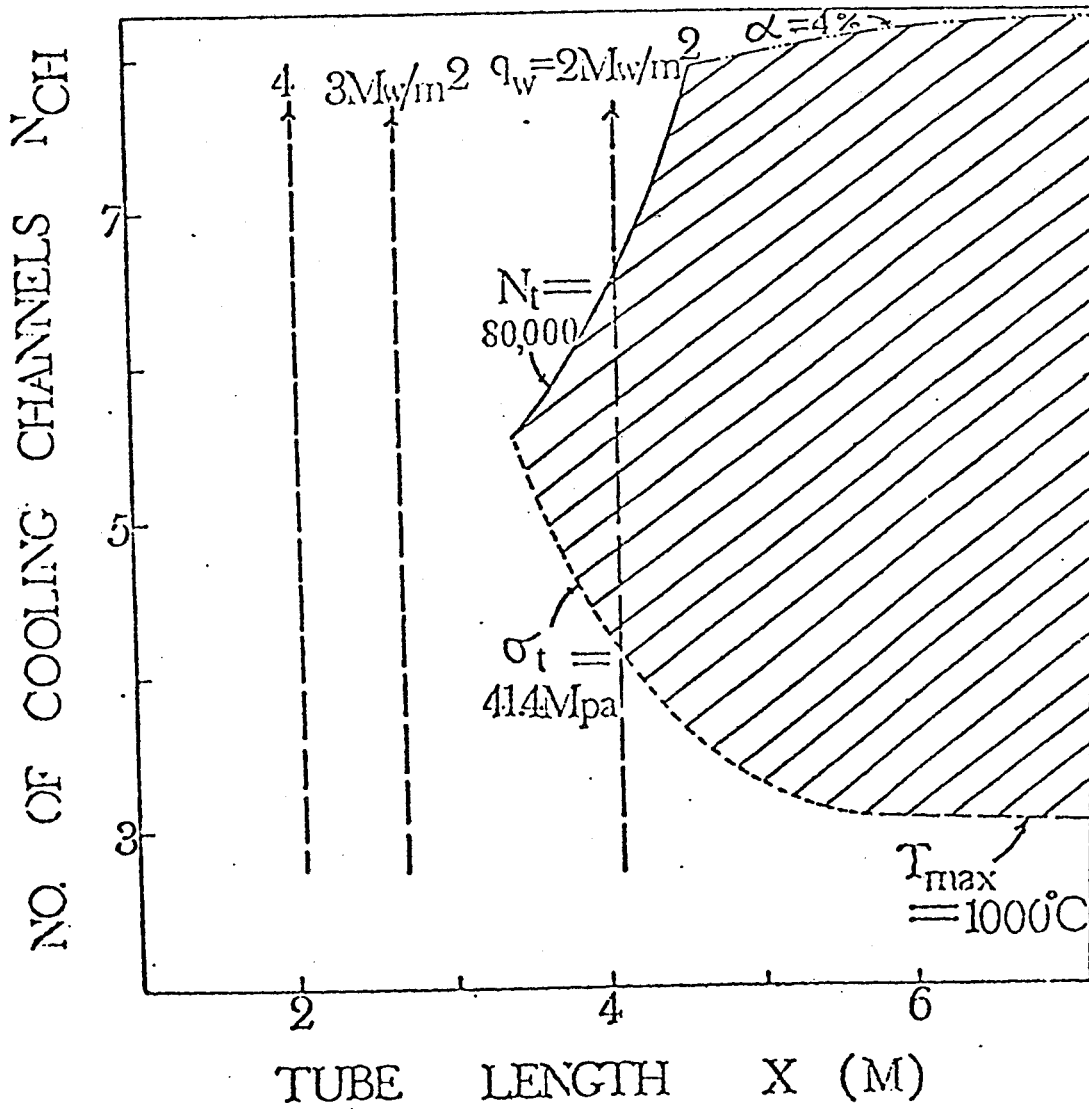


FIGURE 13. THE DESIGN WINDOW OF THE CONSTANT T_{\max} MODEL. THE WINDOW IS BOUNDED BY $\alpha = 80,000$, $\sigma_t = 41.4$ Mpa, AND $T_{\max} = 1000^\circ\text{C}$ LINES. PARAMETERS HELD CONSTANT ARE THE SAME AS THOSE IN FIG. 12.

2.4 Discussion

The major tasks of designing a Tokamak blanket are to identify the potential design constraints, and then to develop configurations which satisfy them. This study has shown so far the methodology to achieve such objectives by analyzing two basic configurations: the constant \dot{Q}' model and the constant T_{\max} model.

As a result of the analysis, the design window of parameters is formed for each model and the most limiting constraints can be identified from it. The formation of a design window is useful in determining the maximum first wall loading for a particular design. Thus, it provides a common basis to compare different designs. The size of the blanket module and the geometry of the coolant passage arrangements can be generally predicted from the window.

Table I shows the comparison of the two design models proposed in this work. The maximum wall power for each model and the design parameters used to reach such maximum power are listed in the table. In the constant \dot{Q}' model, the first wall power is limited by the total number of tubes and the largest size of the headers that can fit in the blanket. The maximum first wall power is found to be about 6 Mw/m^2 . In the constant T_{\max} model, the thermal stress in the coolant channel wall is the limiting constraint, while the header size is fixed at the largest value found in the constant \dot{Q}' model. Because of its lower maximum wall loading, the constant T_{\max} model is considered inferior to the constant \dot{Q}' model.

TABLE I. Comparison of the Two Models

Parameter	Constant \dot{Q}' Model	Constant T_{\max} Model
limiting constraint(s)	total number of tubes = 80,000 and maximum header size = 12.76 cm	thermal stress = 41.4 Mpa
maximum wall loading (MW/m^2)	6	2.1
tube length (m)	1.7	3.7
number of coolant channels or tubes along the header	13	5
pumping power ratio	0.01	0.01
tube diameter (cm)	2.0	2.55
header diameter (cm)	12.76	12.76
inlet coolant velocity (m/sec)	0.1	0.1

It is not the objective of this thesis to arrive at any specific design. The two proposed models are merely used to illustrate the methodology of determining the design window for the design parameters. Neither is it the goal of this work to search for the appropriate values for the design limits. The proper choice of a value for stress limit, for instance, depends upon the success of modelling and obtaining the data on mechanical behavior of structural materials in a simulated CTR environment. A better design window can be easily constructed, from the methodology proposed, by employing the appropriate values for the design limits. Some aspects of these limits are discussed in Chapter 4.

The calculation methods for MHD pressure drops in this study are considered approximate and are used here for the purpose of demonstration. The same methodology can be exercised repeatedly to reach a specific blanket design upon the development of methods which could incorporate the effects of time varying fields or varying crosssection of headers. In this case one could simply recalculate a new value for the safety factor which is introduced in the present approach.

NEUTRONIC CALCULATIONS

3.1. Introduction

A complete neutronic scheme is prepared for calculations of the volumetric heating rate, the breeding ratio, and the radiation damage rates.

The volumetric heating rate as a function of distance from the first wall is required for heat transfer analyses of blanket design. An acceptable breeding ratio limits the allowable quantity of structural material in a blanket, thus establishing an engineering design constraint. The first wall lifetime for a given neutron loading is limited by the radiation damage which degrades the mechanical properties of the material.

Due to the non-uniform heat generation throughout the blanket region, it is desirable to arrange the coolant passages in a non-uniform distribution which matches heat generation thereby reducing the possibility of hot spots. Such arrangements have been discussed in the previous section. To determine the difference in breeding and heating for lithium coolant and different structural distributions, the neutronics in this study extends works reported in the literature where only regionally uniform blankets were considered. (27,28,29)

In the previous section, stainless steel with its low electrical conductivity is used to demonstrate the design models and the associated thermal-hydraulics. In a recent study, 20% cold work 316 stainless steel was also suggested for use as a first wall material in near term tokamak fusion devices (30) and is thus again

to be the first wall material as well as the structural material in the blanket in the neutronic calculations.

A number of computer codes, including ANISN,⁽³¹⁾ ABTR,⁽³²⁾ TAPEMAKER,⁽³¹⁾ NEBULA and RECOIL⁽³³⁾, are used to complete the neutronic scheme. ANISN, a one dimensional discrete ordinates transport code, is used to calculate the flux distributions and breeding ratios. Previous efforts showed that a $P_3 - S_4$ approximation would be adequate when detailed spatial information is not desired.⁽³⁴⁾ In this study, all ANISN runs use a $P_3 - S_4$ approximation.

NEBULA is developed in this work to calculate volumetric heat generation rate in the blanket by inputting Kerma factors, and fluxes calculated by ANISN. NEBULA is also capable of radiation damage calculations using the same fluxes calculated by ANISN, and cross sections for atomic displacements and gas production which are generated by RECOIL. The definition of Kerma and detailed information on NEBULA are documented in Appendix F.

The cross sections for ANISN flux calculations, and the Kerma factors are stored on DLC-37D tape,⁽³⁵⁾ which contains an up-to-date 100 neutron and 21 gamma group data set for fusion reactor materials. Both DLC-37D and RECOIL were obtained from the Radiation Shielding Information Center at Oak Ridge National Laboratory.

ABTR (ANISN Binary Tape Routine) was developed by Franklin Chen in his thesis work.⁽³²⁾ It retrieves and selects the cross sections of the materials needed from DLC-37D for a particular blanket model.

TAPEMAKER helps reduce the storage required for ANISN runs.

ANISN solves neutron and gamma fluxes group by group starting from the first (highest) energy group. Thus, the computer space needed for each ANISN job is greatly decreased with the input of cross sections already ordered by group number. However, the cross sections in DLC-37D are stored in the sequence of material number*. TAPEMAKER was coded to rearrange the cross section in order of energy group and store them on a storage tape. The tape was used regularly for inputting ANISN.

*The material number is defined in Ref. 31 and 35.

3.2. Blanket Model and Calculation Procedures

Three types of blanket configurations are considered. Figure 14 shows the blanket configuration (type A) with a uniform breeding zone. The blanket consists of a 0.5 cm first wall, an 80 cm breeding zone, and a 10 cm graphite zone. Lithium is used as both coolant and breeding material. When structural material is distributed to accommodate a non-uniform heat generation, the blanket configuration in Fig. 15 (type B) is assumed for netronic calculations (to simplify input to ANISN). The value of volume percent structural material is calculated by averaging the values for all breeding zones. To model the effect of varying amounts of structural material in the blanket, x (cf. Fig. 15) is varied from 1.5 to 0.5.

In principle, coolant passages may also be arranged to form coolant channels. The channels can be spaced such that the maximum temperatures between the channels are the same. This has been demonstrated in the constant T_{\max} model in Chap. II. To evaluate this constant T_{\max} regionally homogenized model of the non-uniform distribution of structural material, which we have considered so far, a third type of configuration is used. Figure 16 shows such a configuration (type c), in which six channels are employed and 3 percent of the structural volume is assumed to account for materials used as module walls, grids and supporting elements in the regions between coolant channels.

A 10 cm thick graphite zone is placed for reflection at the blanket's outer edge, and an albedo value is chosen there for all models in this work. In most cases, an albedo of zero is taken to

Distance in c.m.	Zone number	Number of Inter- vals per Zone	Material	Thickness (cm)
0	1	1	Plasma	250
250	2	1	Vacuum	49.5
299.5	3	3	S.S.	0.5
300	4	40	90% Li 10% S.S.	80
380	5	5	C	10
390				

Fig. 14. Configuration of the Blanket (Type A) with Uniformly Distributed Material in the Breeding Region

Distance in cm.	Zone number	Material
0	1	Plasma
250	2	Vacuum
299.5	3	S.S.
300	4	(100-13X)X Li S.S.
320	5	(100-11X)X Li (11X)X S.S.
340	6	(100-9X)X Li (7X)X S.S.
360	7	(100-7X)X Li (7X)X S.S.
380	8	C
390		

Fig. 1.3. Configuration of Blanket (Type D) with Non-Uniformly Distributed Structure in the Breeding Region, Where x Varies from 0.5 to 1.5.

Distance in cm.	250	299.5	300	307.1	316.5	328.1	344.7	377.5	380	390						
Zone Number	1	2	3	4	5	6	7	8	9	10	11	12	13	14	15	
Number of intervals per zone	1	1	3	2	2	2	3	2	4	2	6	2	3	2	5	
Thickness (cm)	250	49.5	0.5	2.55	2.55	2.55	2.55	2.55	2.55	2.55	2.55	2.55	2.55	2.55	10	
Material	plasma	vacuum	S.S.	28% Li	13.6% S.S. 97% Li	13.6% S.S. 97% Li	13.6% S.S. 97% Li	28% Li	13.6% S.S. 97% Li	13.6% S.S. 97% Li	13.6% S.S. 97% Li	13.6% S.S. 97% Li	13.6% S.S. 97% Li	28% Li	13.6% S.S. 97% Li	C

Fig.16. Configuration with 6 Coolant Channels in Breeding Zone (Type C)

ensure a conservative estimate of breeding. Some ANISN runs with albedo values of 1 and 0.45 are also executed to examine the effect on breeding and heating. Cylindrical geometry is employed for all ANISN calculations. Table II give the nuclide densities of consitutent material used. (36,37)

The high cost of running ANISN with 100 neutron groups (see Ref. 35 for group structure) is the incentive for seeking a calculational procedure which uses fewer groups. The cross sections using fewer groups are obtained by running an ANISN case of 100 neutron and 21 gamma groups in a group collapsing mode. A previous study (38) concluded that 20 neutron group calculations were appropriate for blanket neutronics. Use of 20 neutron groups could reduce the cost by a factor of 30 provided a few benchmark cases with 100 neutron and 21 gamma group are run. The calculations for a blanket using lithium as coolant can be successfully performed in 20 neutron and 6 gamma groups. Table III shows the reduced group structure.

The overall scheme for the neutronic calculations is shown in Fig. 17.

Stainless Steel 316		Natural Lithium		Flibe		Graphite	
Ni	0.00985	Li ⁶	0.00344	Li ⁶	0.00175	C	0.0804
Cr	0.01575	Li ⁷	0.04296	Li ⁷	0.02185		
Fe	0.05642			Be	0.01215		
Mn	0.00175			F	0.04790		
Mo	0.00126						

TABLE II. Summary of Nuclide Densities (atoms/cm³ x 10⁻²⁴)

	GROUP NUMBER	E_{\max} (MeV)	E_{\min} (MeV)
Neutron	1	14.918	13.4999
	2	13.499	12.214
	3	12.214	2.4082
	4	2.4082	4.0657
	5	4.0657	2.2313
	6	2.2313	1.2246
	7	1.2246	0.67206
	8	0.67206	0.40762
	9	0.40762	0.30197
	10	0.30197	0.22371
	11	0.22371	0.16573
	12	0.16573	0.12277
	13	0.12277	0.67379
	14	0.067379	7.1017×10^{-3}
	15	7.1017×10^{-3}	7.4852×10^{-4}
	16	7.4852×10^{-4}	7.8893×10^{-5}
	17	7.8893×10^{-5}	8.3153×10^{-6}
	18	8.3152×10^{-5}	8.7642×10^{-7}
	19	8.7642×10^{-7}	5.3158×10^{-7}
	20	Thermal	
Gamma	21	14	12
	22	12	10
	23	10	8
	24	8	5
	25	5	2
	26	2	0.01

TABLE III. 26 Energy Group Structure

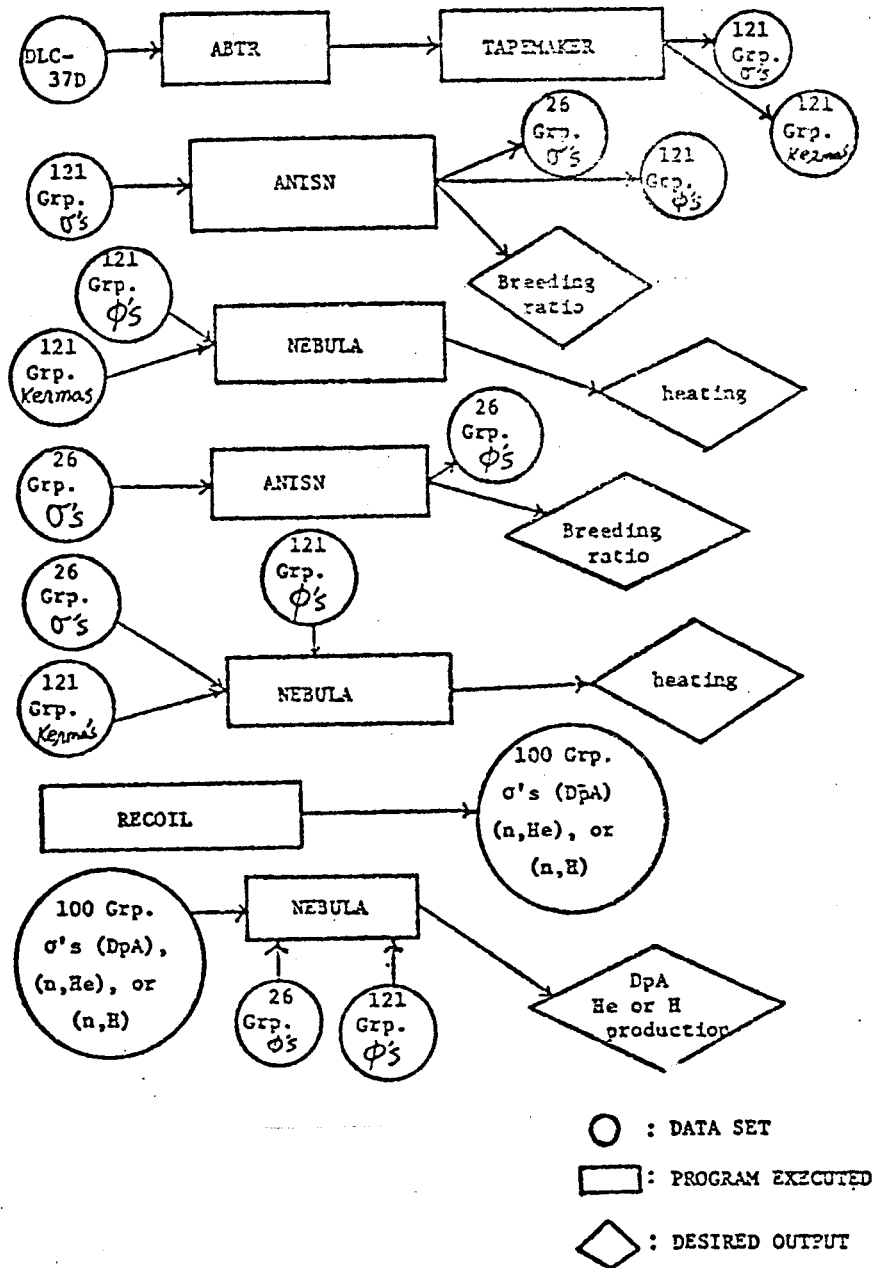


FIGURE 17. FLOW CHART FOR NEUTRONIC CALCULATIONS

In order to check ANISN calculations in this study, the benchmark fusion blanket problem is solved. The breeding ratio is in good agreement with published value.⁽³⁹⁾ The volumetric heat generation similar to published work done with ANISN in slab geometry⁽²⁷⁾ is produced by NEBULA using kerma factors from DLC-37D and a flux distribution generated by ANISN in cylindrical geometry.

To ensure the proper use of the 26 group structure, both 121 group and 26 group calculations are performed once for each blanket configuration. Some calculated breeding ratios presented in Table IV show that the few group structure adopted here is appropriate (c.f. cases 1 and 3). Figure 18 shows the heat flux as a function of distance from the first wall as calculated by NEBULA for a lithium cooled blanket with 5% stainless steel non-uniformly distributed. Both 121 group and 26 group calculations are done by ANISN. The difference is insignificant.

The albedo value of zero for each energy group is used to give conservative estimates on breeding in all but two cases (Table IV) which are used to check the effect of albedo value on breeding. In Table IV, cases 2, 4, and 6 use albedo values of 0.045, 1, and 0, respectively. It was suggested that an albedo of 0.45 would be adequate for blanket models with a short reflector.⁽⁴⁰⁾ The error introduced by using an albedo of zero, comparing cases 2 and 6, is approximately 1.5%. The volumetric heat generation rates for the two cases are shown in Fig. 19. Except near the reflector, the heating curves

Case	Coolant Used	Structure Fraction	Energy Group	Blanket Type	Albedo Value	Breeding Ratio
1	Li	5%	121	B	0	1.481
2	Li	10%	26	B	0.45	1.368
3	Li	5%	26	B	0	1.481
4	Li	10%	26	B	1	1.463
5	Li	15%	26	B	0	1.256
6	Li	10%	26	B	0	1.351
7	Li	10%	26	A	0	1.402
8	Li	5%	26	D	0	1.474

TABLE IV. Breeding Ratios of Various Blanket Configurations
and Different Coolants

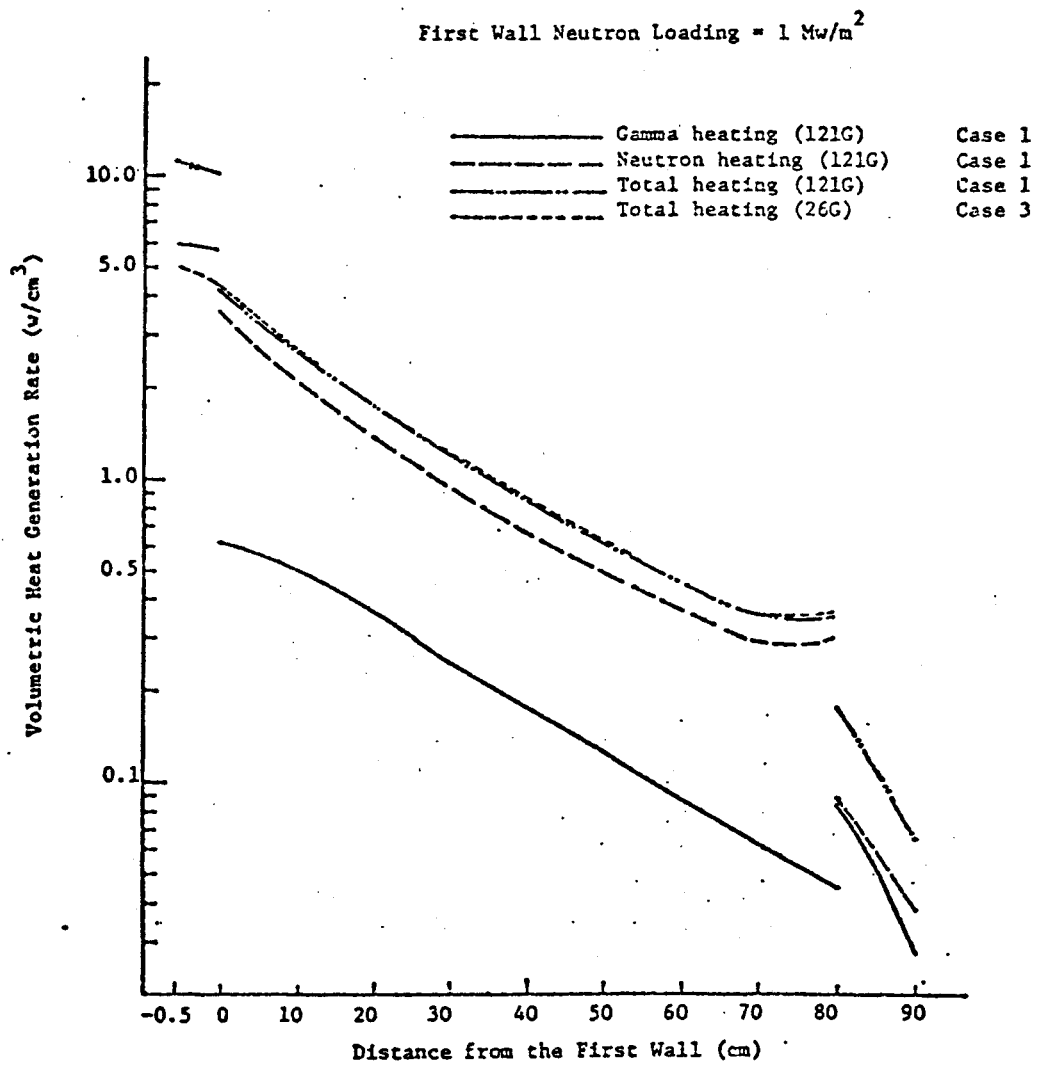


Fig.18. The Comparison of Heating Rates Using Different Group Structures

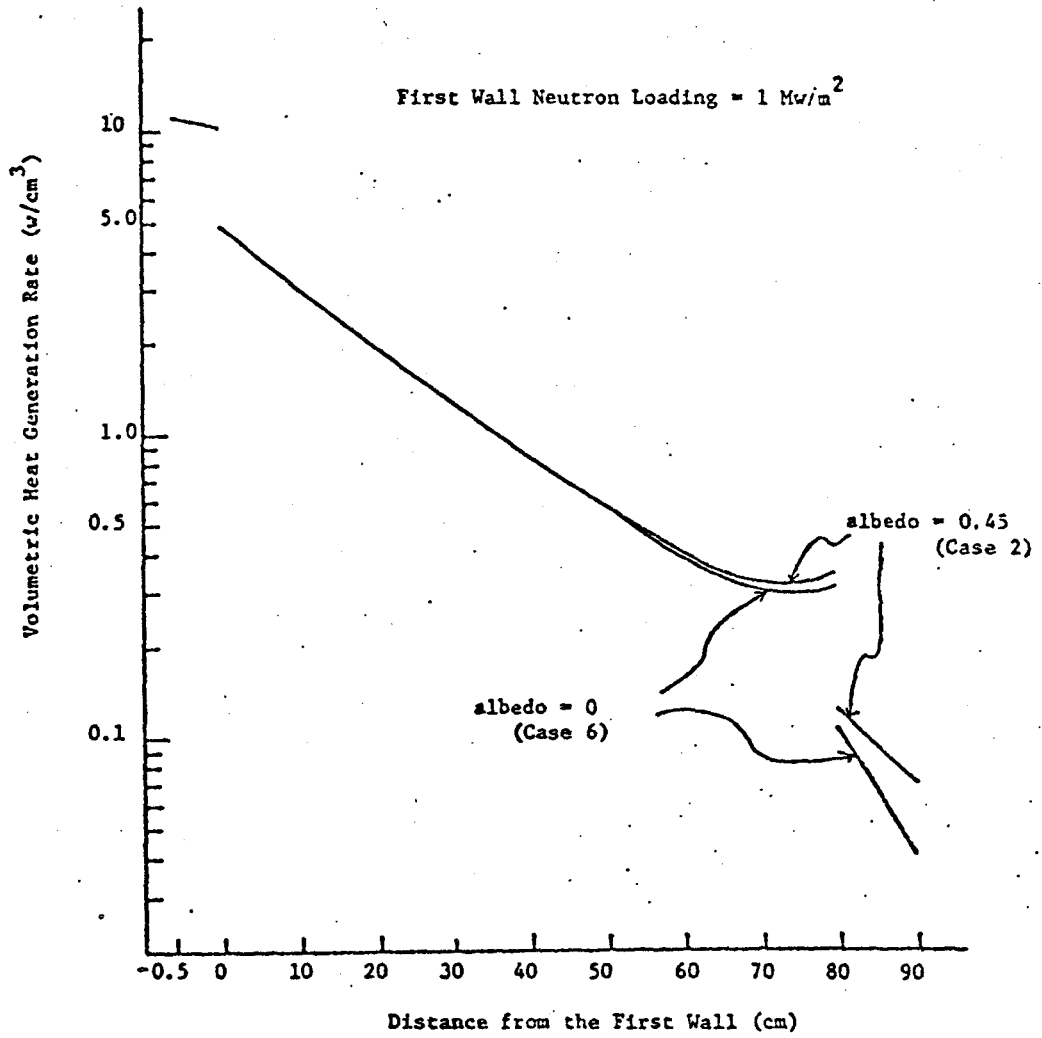


Fig.19. The effect of Using Different Albedos on Heating

in the breeding region coincide. The objective of comparing the two cases is to show the change in heating caused by assuming an albedo of zero for lithium cooled blankets.

Figure 20 shows the breeding curves for lithium coolant as a functions of structural volume fraction in the breeding zone. The dotted line represents results published for UWMAK-I, which uses a blanket with a 58 cm breeding zone, and is different from the configurations employed in this study. Other breeding curves for helium-and flibe-cooled systems are also shown in the figure. The details of the helium-and flibe-cooled blanket configurations are shown elsewhere.⁽⁴¹⁾ From these curves, the lithium-cooled design seems more attractive than those using flibe or helium as coolant, with the same amount of structural material (stainless steel) present.

In Table IV, comparing case 3 and 8, and cases 6 and 7, we conclude that the error in breeding due to different structural distributions or arrangements is within an acceptable range, and is less than the error due to an uncertainty in the partial cross sections of lithium.⁽³⁹⁾

For the simplicity of the analysis, the use of lead, beryllium or their compounds has not been considered, although several studies^(42,43) have demonstrated the merits of using them for neutron multiplication purposes. From a recent study⁽⁴²⁾, the minimum thickness of a blanket can be found through optimization procedures for a specific design. However, seeking a minimum thickness is not the goal of this study; instead, the thickness of the breeding zone is held constant at 80 cm to illustrate the neutronic performance of blankets to support

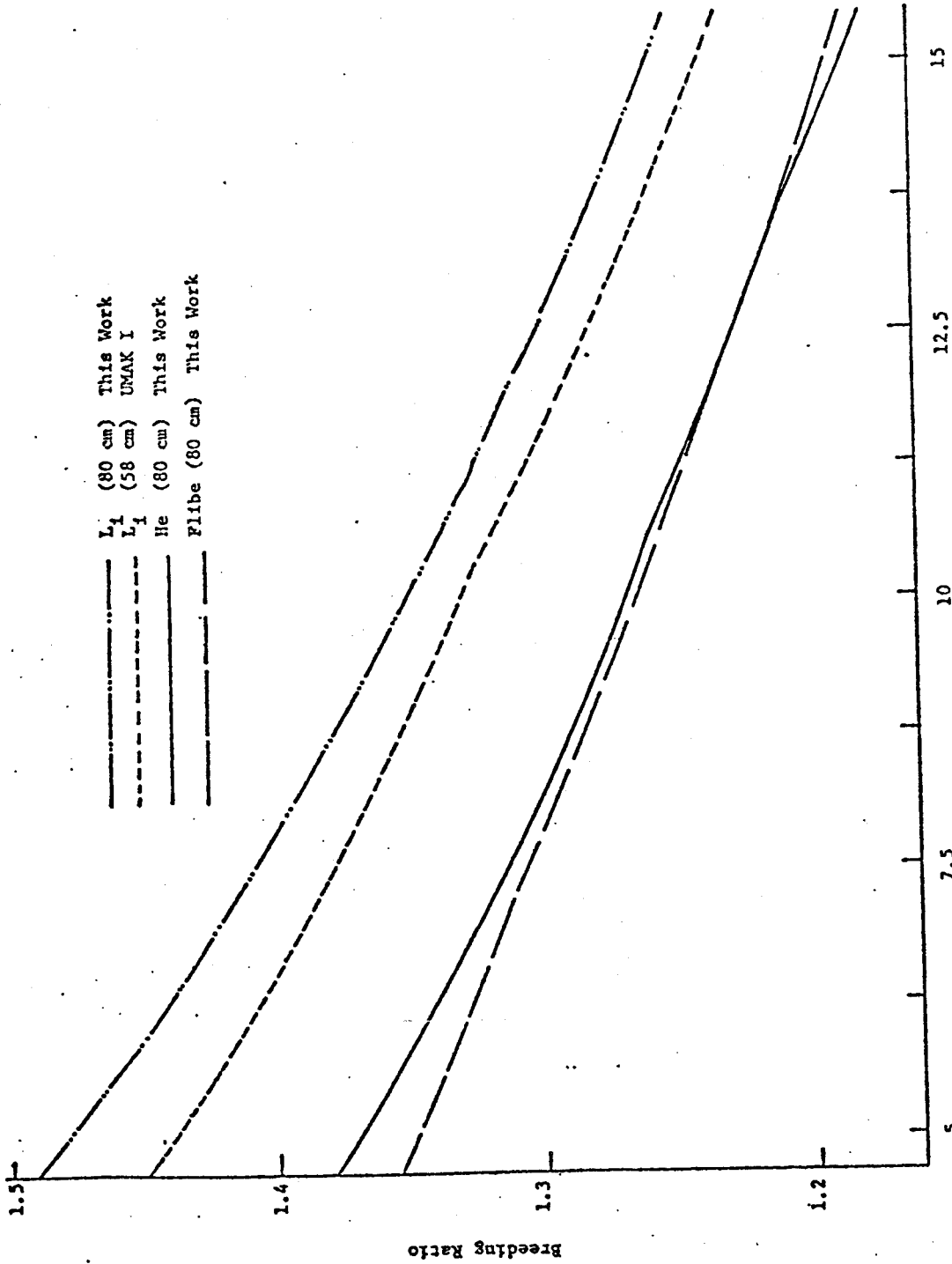


Fig.20. Breeding Ratios as Functions of the Amount of Structural Material in Breeding Zone for Helium, Flibe, and Lithium as Coolants

the thermal-hydraulic analysis.

The displacement per atom and gas production rates have been calculated for Type 316 stainless steel at the first wall of blanket configuration type B (Fig. 15). The results and the comparison with other works are shown in Table V. The only other works on such calculations were done at University of Wisconsin⁽⁴⁴⁾ and Oak Ridge National Laboratory.⁽⁴⁵⁾ The reasons for the slight discrepancies among their results are also listed in the table.

Differences in ENDF/B-III⁽⁴⁶⁾ and ENDF/B-IV⁽⁴⁷⁾ (ENDF stands for Evaluated data file) cause discrepancies between the calculations done by the University of Wisconsin and Oak Ridge. In the Oak Ridge tokamak reference design, a 3 mm graphite curtain is placed on the first wall⁽⁶⁾ and will give a neutron spectrum different from that of a bare first wall. The discrepancies between Oak Ridge's results and this work is due to such differences in the spectra.

Although, only examples are shown for the calculations of radiation damage in the first wall, NEBULA can calculate the displacement per atom and gas production rate as a function of position anywhere in the blanket.

Source	Displacement Damage (dpa/a) ($\times 10^{-7}$)	Helium (appm/s) ($\times 10^{-7}$)	Hydrogen (appm/s) ($\times 10^{-7}$)	First** Wall Design	Cross** Sections Used
This Work	4.0	51	161	bare wall	From ENDF/B-IV
Ref. 44	3.1	64	170	bare wall	From ENDF/B-III
Ref. 45	3.6	46	169	with 3mm graphite curtain	From ENDF/B-IV

TABLE V. Radiation Damage Rates in Type-316 Stainless Steel
as the First Wall Material*

*Neutron Wall loading = $1 \text{ Mw}/\text{M}^2$

**Reasons responsible for the difference in the results

CHAPTER IV.

INTERACTIONS BETWEEN THERMAL-HYDRAULICS AND NEUTRONICS

4.1. Design Procedures

The overall design procedures incorporating both thermal-hydraulics and neutronics studies are summarized below:

1. Define the physical dimensions of the blanket to be considered. Choose inlet temperature and temperature rise of lithium coolant.
2. Choose a design model. In this work, two configurations for the tubes have been proposed in Chapter II: the constant \dot{Q}' model and the constant T_{\max} model.
3. Determine the liquid lithium velocity at the header inlet. Section 2.1 discusses the significance of this parameter. The derivation of the upper limit on U_H is given in Appendix C.
4. select a \dot{Q}''' , the volumetric heat generation rate, as a function of the distance from the first wall; for a stainless steel blanket, the following expression is used (described in Chapter III)

$$\dot{Q}''' = 24.67 e^{-0.042Y} \quad (\text{w/cm}^3)$$

5. For a given number of cooling channels or tubes between two headers, determine the tube positions by satisfying the constant \dot{Q}' condition in the constant \dot{Q}' model, or the channel positions by satisfying the constant T_{\max} condition in the constant T_{\max} model.

6. Calculate a new \dot{Q}''' based on the structural distribution proposed in Step 5.
7. Repeat Step 5, using the new \dot{Q}''' from Step 6.
8. If the tube or channel positions determined in Step 7 are not the same as those obtained in Step 5, go to Step 5. Repeat Steps 5 and 6, until the tube or channel positions are the same as those obtained in the previous iteration, or the differences between the two sets of positions are within an acceptable range.
9. Calculate the peak temperatures in the stagnant lithium pool as a function of distance from the first wall by solving the conduction equation. The calculational methods are given in Appendix B.
10. Select a value for N such that the hot spot is away from the first wall.
11. Calculate $D_{H_{\max}}$ corresponding to N chosen in Step 10.
12. Choose an upper bound on the peak temperature in the lithium pool based on the limit of the vapor pressure of lithium at high temperature, or the temperature limit on the mechanical properties of the materials used as module container walls, grids, or supporting elements.
13. Calculate radiation damage rates in the structural material.
14. Determine the limit on the stress level. It will be a function of radiation damage rates obtained from

Step 9, and the cycling characteristics of the power generation.

15. Choose a limit on N_t . To increase the reliability of a cooling system, a low number of weld joints is desirable. The number of weld joints is proportional to the number of tubes. Therefore, a limit on tube number must be specified. Reference (48) provides a method to estimate such limit.
16. Determine the upper bound on α , the fraction of structural material in the blanket, based on the breeding ratio achieved by such a blanket. Breeding ratios of more than 1.15 are desirable.⁽⁴⁹⁾ It is necessary to breed more than one triton per triton burned because of the loss of tritium by radioactive decay, and because of losses in plant holdup tanks, and in recovery and recycling operations.
17. Obtain design windows from thermal-hydraulic analyses. In this work, codes BEER-CAN and WINDOW have been used in the constant T_{\max} model and constant Q' model, respectively. Results given in Steps 11, 12, 14, 15 and 16 are required to define the window.
18. From the design window, the maximum first wall neutron loading of the system is identified and the dimensions associated with the cooling modules are deduced. Other results include the pumping power to heat removal ratio, tube and header thicknesses, and coolant velocities in the channels.

4.2. Interactions Between Thermal-Hydraulics and Neutronics

Strong interactions exist between neutronics and thermal-hydraulics. This fact can be observed in Step 5 through 8 in the previous section. The cooling channel arrangements depend on the neutronic calculations and vice versa. However, the volumetric heat generation is insensitive to the material distributions adopted in this study; hence, convergence could be reached in one or two iterations. Nevertheless, only the demonstration of the design methodology is presented here; therefore, no iterative process has been attempted in this work due to the high computer cost of using DLC-37D and ANISN.

One assumption has been made to obtain U_H in Step 3. A coating layer of electrical insulation material on the surface of cooling tubes is assumed. Since no existing insulation material has demonstrated the chemical compatibility with the stagnant lithium in the blanket, another layer of stainless steel over the insulation material must be used to prevent direct contact with lithium. This additional amount of stainless steel implies a decreased breeding ratio. The purpose of using the electrical insulation layer is to prevent the electrical current from leaking into the lithium pool. Any current leakage would result in a higher voltage drop across the cooling tubes and thus would cause higher MHD pressure drop. The neutronic performance with the presence of the insulation material is unknown. Thus, the breeding ratio calculated in Step 16 serves as a limit on the quantity of structural material required to cool the blanket and has an indirect impact on the pressure drop.

The limit on stress level of the material is a function of radiation damage rates and other thermal and mechanical parameters. Radiation damage rates calculated by neutronic codes in this work include displacements per atom, helium production rate, and hydrogen production rate. The high helium production rate caused by the reactions of steel with 14-MeV neutrons generated in a fusion reactor is more significant than that in a fission reactor. Loss of ductility, swelling, and possible reduction in fatigue resistance are enhanced by the helium production. Yet, no data or theoretical model which accounts for helium effects is available to predict the limit on stress for chosen lifetime of the material. Thus, studies on the effects of neutron interactions on material properties are needed to provide information on the design limit for the thermal hydraulic models. In this study, a stress limit based on fission data is used to demonstrate the overall design methodology.

4.3. First Wall Considerations

For each fusion reaction a 3.5-MeV alpha particle and a 14-MeV neutron are produced. Neutrons penetrate through the first wall and convert their kinetic energy into sensible heat in the blanket region. Alpha particles with much less penetrating power are stopped by the first wall and hence impose a high surface heat flux to the wall. Such heat flux may cause high temperature and high thermal stress in the wall. The pulsing nature of the fusion power may create fatigue problems in wall material. High radiation damage rates will occur in the material due to the bombardments with neutrons of high energies, and will degrade the mechanical properties of the material. The volumetric heat generation rate in the wall is more than twice as high as that in the blanket region behind the wall. Thus, the cooling of the first wall requires different design strategies due to the complexity associated with the thermal-hydraulics, neutronics, and the interactions between them. A set of design constraints different from those for the rest of the blanket are imposed. Such constraints may vary from one specific design to another and are difficult to generalize. Therefore, the first wall should be considered separately from the rest of the blanket. In this work, we have assumed that the surface heat flux from the plasma to the first wall has been removed by a separate cooling system.

The methodology developed in this study can be used to predict the maximum first wall loading with the constraints satisfied by the blanket parameters. For example, a maximum first wall loading

of 6 Mw/m^2 can be achieved by the constant \dot{Q} configuration (described in Chapter II). However, the integral lifetime (defined as $\lambda \cdot q_w \text{ yr} \cdot \text{Mw/m}^2$) is limited by the loss of ductility of the material caused by radiation damage rates based on fission data. An upper bound on the integral lifetime was found $2\text{-}3.5 \text{ yr Mw/m}^2$. (26,50)

A blanket operated at 6 Mw/m^2 wall loading will then have a lifetime for the first wall less than 0.5 year. Such design is not economically attractive to reach an optimum design. The methodology presented in this study should be incorporated to the first wall cooling system considerations.

SUMMARY, CONCLUSIONS AND RECOMMENDATIONS

5.1. Summary

A complete design methodology for a lithium cooled tokamak blanket has been developed which determines acceptable ranges for design parameters. Two design models illustrate the thermal-hydraulic portion of the methodology. One model is a constant \dot{Q}' model, and the other, a constant T_{\max} model. In both models, tubes are arranged parallel to the toroidal field to minimize MHD pressure drops, and headers oriented perpendicular to the field are used to deliver the lithium coolant. In the constant \dot{Q}' model, tubes are spaced so that each tube will receive an equal amount of heat. In the constant T_{\max} model, tubes are concentrated at several radial positions to form coolant channels. The channel positions are so chosen that the maximum temperatures between the channels are equal.

To obtain acceptable ranges for design parameters (design window), the principles of conservation of energy, conservation of mass, and conservation of momentum must be satisfied as well as all other thermal-hydraulic constitutive relations. The parameters considered are first wall neutron loading, coolant channel length, cooling tube and header diameters, thicknesses of tubes and headers, number of tubes, number of sectors, and coolant velocities. The constraints on a blanket design include an upper bound on pumping power, stress level, temperature, fraction of structural material in the blanket and number of tubes. A comparison of the two models has been made.

The methodology demonstrated by the two models can be used to identify the limiting constraints for a particular design. The size of the blanket module and the geometry of the coolant passages can be deduced from the design window. The design methodology may be used in general for different choices of structural materials, reactor dimensions, or magnetic field strength, in the analysis of a hypothetical reactor.

A complete neutronic scheme has been prepared for the calculation of the volumetric heating rate as a function of the distance from the first wall, the breeding ratio as a function of the amount of structural material in the blanket, and the radiation damage in terms of displacements per atom and gas production rates.

A non-uniform distribution of structural material is modeled by choosing different volumetric percentages of 316 stainless steel in several breeding zones, while still satisfying thermal-hydraulic requirements for the two models. The effect of using different albedo values at the outer edge of each blanket configuration has been examined in this study. The role that the radiation damage plays in the overall design methodology has been presented and discussed.

5.2. Conclusions

1. The fraction of structural material in the blanket does not impose a design constraint for the cases considered, because of the high breeding ratios achieved by a lithium blanket.
2. The pumping power required for a lithium cooled system is low. The pumping power ratio (C_p) is typically equal to or less than 0.01.
3. For the constant \dot{Q}' model, the design constraints are the total number of tubes and the maximum header size that can fit radially in the blanket. The maximum first wall loading for this model is 6 Mw/m^2 .
4. Thermal stress is the constraining factor in the constant T_{max} model. The maximum first wall loading for this model is 2.1 Mw/m^2 .
5. For an average volumetric fraction of stainless steel in the blanket of 0.05, the difference in breeding ratio between the constant \dot{Q}' model and the constant T_{max} model is less than 1%.
6. The difference in breeding ratio where the albedo value is changed from 0.0 to 0.45 is 1%.
7. The effects that different structural distributions and albedo values have on heat generation rate are insignificant.
8. The lithium coolant velocity at the header inlet should be equal to or less than $U_{H,\text{crit}}$ (eq. 1), to avoid exceeding

a reasonable hoop stress. A typical value for $U_{H,crit}$ is 0.1 m/sec.

9. For a coolant inlet velocity less than $U_{H,crit}$, the header and tube thicknesses are limited only by corrosion and fabricability considerations, and may be as thin as practical.

5.3. Recommendations

At the conclusion of this study, several areas which would benefit from further study are identified.

An additional heat flux is generated due to the impact of the charged particles upon the first wall. A separate design study for transferring the surface heat flux on the first wall is needed. The design limits considered in this case include an upper bound on the temperature, thermal stresses, and wall lifetime. The wall lifetime is limited by the degradation of material properties due to radiation damage rates, and fatigue resistance of the material.

Within the stagnant lithium region, the free convection will have effect on heat removal. The interactions of MHD forces with the buoyant forces in the stagnated lithium region should be investigated. This additional heat transfer reduces the maximum temperature, which may be a design limit.

A three dimensional heat conduction analysis should be performed for the blanket, in order to determine more accurately the temperature distribution.

A serpentine tube arrangement between the inlet and outlet headers will increase the length of the tubes and thus decrease the total number of tubes (c.f. figure 21). The total number of tubes is a design limit in this study. Therefore, serpentine tube configurations should be examined in further design studies.

The blanket thickness has been assumed to be constant in this work. The neutronic scheme could incorporate optimizing procedures that seek a minimum blanket thickness within the limits of acceptable

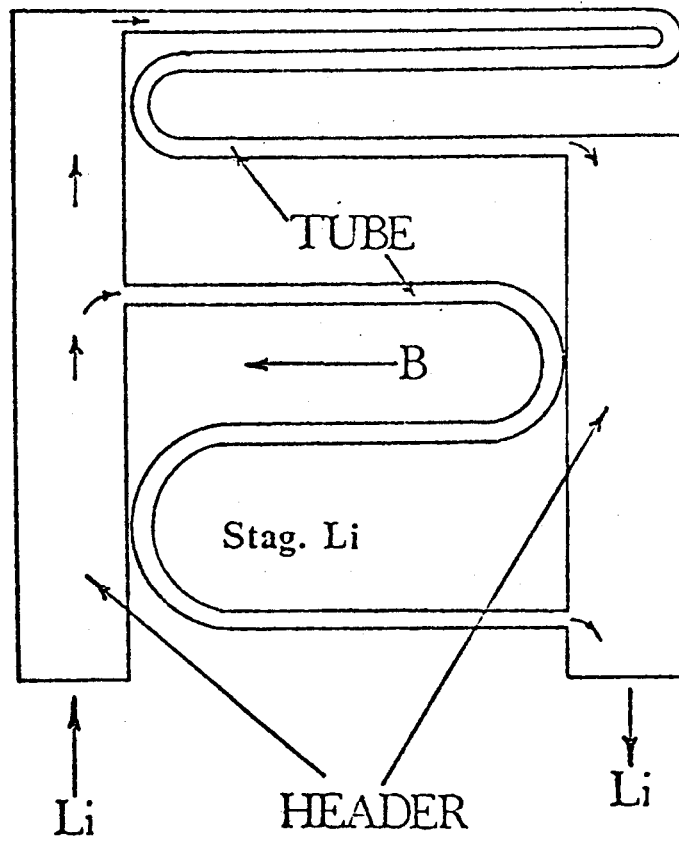


Figure 21. A serpentine tube arrangement.

breeding ratio, shielding effectiveness, and energy multiplication.

For fusion reactor blanket, a method to estimate the design limit on the stress level is needed. This limit should be a function of helium production rate, atomic displacements, temperature, the pulsing nature of the heat flux passing through the material, and the specified lifetime of the material. The lifetime of the material is limited by certain failure criteria, such as strain and swelling.

REFERENCES

1. J. Chao, graduate student, nuclear engineering; T.J. McMamanamy, graduate student, nuclear engineering; B.B. Mikić, professor, mechanical engineering; and N.E. Todreas, professor, nuclear engineering.
2. B.G. Twing, Division of Magnetic Fusion Energy, ERDA, and J.R. Powell, Brookhaven National Laboratory, "An Assessment of Blanket and Shield Technology."
3. G.L. Kulcinski, "Major Technological Problems for Fusion Reactor Power Stations," University of Wisconsin, November, 1972.
4. A.P. Fraas, "Comparative Study of the More Promising Combinations of Blanket Materials, Power Conversion Systems and Tritium Recovery and Containment Systems for Fusion Reactors," ORNL-TM-4999, November, 1975.
5. "Tokamak Experimental Power Reactor Conceptual Design," ANL/CTR-76-3, August, 1976.
6. "Oak Ridge Tokamak Experimental Power Reactor Study," ORNL-TM-5572, September, 1976.
7. "Experimental Fusion Power Reactor Conceptual Design Study," GA-A 14000, July, 1976.
8. J.C.R. Hunt and R. Hancox, "The Use of Liquid Lithium as Coolant in a Toroidal Fusion Reactor," CLM-R115, October, 1971.
9. "UWMK-I, A Wisconsin Toroidal Fusion Reactor Design," UWFD-68, March, 1974.
10. "UWMK-II, A Conceptual Tokamak Power Reactor Design," UWFD-112, October, 1975.
11. "UWMK-III, A Noncircular Tokamak Power Reactor Design," EPRI-ER-368, July, 1976.
12. D.G. McAlees, et al., "The Elmo Bumpy Torus Reactor Reference Design," ORNL-TM-5669, November, 1976.
13. B. Misra and V.A. Maroni, "Thermal Hydraulic Analyses of Two Fusion Reactor First Wall/Blanket Concepts," Proceedings of the Seventh Symposium on Engineering Problems of Fusion Research, IEEE pub. No. 77CH1267-4NPS (1977), p. 1459.
14. B. Misra, H.C. Stevens, and V.A. Maroni, "Thermal Hydraulic and Power Cycle Analyses of Liquid Lithium Blanket Designs," Proceedings of the 1977

- National Heat Transfer Conference, August, 15-17, 1977, Salt Lake City, Utah; ASME pub. No. 77-HT-84, 1977.
15. W.M. Wells, "ORNL Fusion Power Demonstration Study: Lithium as a Blanket Coolant," Oak Ridge National Laboratory Report ORNL/TM-6214, April, 1978.
 16. S. Globe, "The Effect of a Longitudinal Magnetic Field on Pipe Flow of Mercury," J. of Heat Transfer, Trans. ASME, 445, 1961.
 17. F.W. Fraim, "The Effect of a Strong Longitudinal Magnetic Field on the Flow of Mercury in a Circular Tube," Ph.D. Thesis, M.I.T., 1966.
 18. A.L. Loeffler, A. Macuilatis, and M. Hoff, "MHD Round Pipe Flow Experiments, USAF-ARL Rept. 67-0236, 1967.
 19. R.A. Gardner and P.S. Lykoudis, "Magneto-Fluid-Mechanic Pipe Flow in a Transverse Magnetic Field with and without Heat Transfer," AIAA paper 69-723, June, 1969.
 20. A.L. Jaumotte and C. Hirsch, "Ecoulement Magnétohydrodynamique en Conduites," *Mechanique Appliquée*, 960, 1967.
 21. R.M. Lyon, ed., "Liquid Metal Handbook," Sponsored by Committee on the Basic Properties of Liquid Metals, Office of Naval Research, Department of the Navy, in Collaboration with USAEC and Bureau of Ships, Department of the Navy, June, 1952.
 22. R.A. Gardner, "Laminar Pipe Flow in a Transverse Magnetic Field with Heat Transfer," J. of Heat Mass Transfer, 11, pp. 1076-1081, 1968.
 23. K.J. Lasky, "MHD Pressure Drop in Flow Around A Corner in a Magnetic Field at High Hartmann Number," M.S. Thesis, Department of Nuclear Engineering, M.I.T., 1977.
 24. Don Steiner, et al., "ORNL Fusion Power Demonstration Study: Interim Report," ORNL/TM-5813, March, 1977.
 25. M.A. Hoffman and G.A. Carlson, "Calculation Techniques for Estimating the Pressure Losses for Conducting Fluid Flow in Magnetic Fluid," USAEC Rept. UCRL-51010, Lawrence Radiation Laboratory, 1971.
 26. R.F. Mattas and D.L. Smith, "Models for Life-Limiting Properties of Fusion Reactor Structure Materials," *Nuclear Technology*, Vol. 39, July, 1978.
 27. D. Steiner, "The Nuclear Performance of Fusion Blankets," *Nuclear Applications and Technology*, Vol. 9, 1970.
 28. D.M. Gruen, ed., "The Chemistry of Fusion Technology," Plenum Press, 1972.

29. M.A. Abdou and C.W. Maynard, "Neutronic and Photonics Design for CTR Blankets and Shields," University of Wisconsin, FDM67, 1973.
30. E.E. Bloom, F.W. Wiffen, et al., "Temperature and Fluence Limits for a Type 316 Stainless Steel CTR First Wall," Nuclear Technology, Vol. 31, October, 1976.
31. W.W. Engle, Jr., "A User's Manual for ANISH, a one Dimensional Discrete Ordinates Transport Code with Anisotropic Scattering," Rept. K-1693, Computing Technology Center, Union Carbide Corporation (1957).
32. Frank Chen, "Thermal and Hydraulic Considerations for the Designing of a Solid Tokamak Blanket," Sc.D. Thesis, M.I.T., May, 1976.
33. T.A. Gabriel, J.D. Amburgey and N.M. Greene, "Radiation Damage Calculations: Primary Recoil Spectra, Displacements Rates, and Gas-Production Rate," ORNL/TM-5150, March, 1976.
34. D. Steiner, "Analysis of a Bench-Mark Calculation of Tritium Breeding in a Fusion Reactor Blanket," ORNL/TM-4177, April, 1973.
35. W.E. Ford, III, R.T. Santoro, R.W. Roussin, and D.M. Plaster, "Modification Number One to the Coupled 100r-218 Cross Section Library for EPR Calculations," ORNL/TM-5249, March, 1976.
36. A.J. Impink, Jr., "Neutron Economy in Fusion Reactor Blanket Assemblies," Tech. Rept. 434, M.I.T., Research Laboratory of Electronics (1965).
37. Reactor Handbook, 2nd ed., Vol. 1, Materials, Tipton, C.R., Jr., Ed., p. 621, Interscience Publishers, Inc., New York, N.Y. (1960).
38. A.G. Cook, "The Feasibility of U^{233} Breeding in D-T Fusion Devices," Engineer Thesis, M.I.T. Nuclear Engineering Department, May, 1976.
39. M. Tobias and D. Steiner, "Additional Results Concerning Cross Section Sensitivity of Tritium Breeding in a Fusion Reactor Blanket: Effects of Cross Sections of Li^6 , Li^7 and Nb^{93} ," ORNL/TM-4201, January, 1974.
40. M. Abdou, Argonne National Laboratory, Personal Communication (December 5, 1977).
41. J. Chao, B.B. Mikić, and N.E. Todreas, "Neutronic Performance of Fusion Reactor Blankets with Different Coolants and Structural Arrangements," Submitted for publication in Nuclear Technology, August, 1978.
42. S.A.W. Gerstl, "A Minimum-Thickness Blanket/Shield With Optimum Breeding and Shielding Effectiveness," The Technology of Controlled Nuclear Fusion, p. 77, Transaction of the Third Topical Meeting, Santa Fe, May, 1977.

43. R. W. Conn, G.L. Kulcinski, and C.W. Maynard, "NUMAK: An Attractive Reactor for the Main Line of Tokamaks," *The Technology of Controlled Nuclear Fusion*, p. 351, Transaction of the Third Topical Meeting, Santa Fe, May, 1977.
44. G.L. Kulcinski, D.G. Doran, and M.A. Abdou, "Comparison of Displacement and Gas production Rates in Current Fission and Future Fusion Reactors," *Properties of Reactor Structural Alloys After Neutron or particles Irradiation*, ASTM-STP-570, p. 329, American Society for Testing and Materials (1975).
45. T.A. Gabriel, B.L. Bishop, and F.W. Wiffen, "Calculated Atom Displacement and Gas production Rates of Materials Using a Fusion Reactor First Wall Neutron Spectrum," *Nuclear Technology*, Vol. 38, May, 1978.
46. O. Ozer and D. Garber, "ENDF/B Summary Documentation," (for ENDF/B-III) BNL-17541 (ENDF-201), Brookhaven National Laboratory (1972).
47. Radiation Shielding Information Center, Private Communication (Summary documentation for ENDF/B-IV to be published).
48. A.P. Fraas, "Comparative Study of the More Promising Combinations of Blanket Materials, Power Conversion Systems, and Tritium Recovery and Containment Systems for Fusion Reactors," ORNL/TM-4999, November, 1975.
49. D.J. Rose, "On the Feasibility of Power by Nuclear Fusion," ORNL/TM-2204, May, 1968.
50. G.L. Kulcinski, et al., "Radiation Damage Fusion Limitations in the Design of the Wisconsin Tokamak Fusion Reactor," *Nuclear Technology*, Vol. 22, April, 1974.
51. R.J. Holroyd, "Magnetohydrodynamic Duct Flow in Non-Uniform Magnetic Field," Ph.D. Dissertation, University of Cambridge, December, 1975.
52. M.A. Hoffman and G.A. Carlson, "Calculational Techniques for Estimating the Pressure Losses for Conducting Fluid Flows in Magnetic Fluid," USAEC Rept. UCRL-51010, Lawrence Radiation Laboratory, 1971.
53. H.F. Carslaw and J.C. Jaeger, "Conduction of Heat in Solids", 2nd Ed., Oxford University Press, 1959.

APPENDIX A: CALCULATIONAL TECHNIQUES FOR
MHD PRESSURE DROPS

The calculation methods for the total pressure loss discussed in Sec. 2.1. are presented in this appendix. The friction pressure loss is insignificant compared with other contributing terms and hence is neglected here.

The pressure drop in the header due to the perpendicularity of the flow to the B field is calculated by the following equation:

$$\Delta p_H = Z \frac{\mu U_H}{\frac{D_H^2}{4}} \left\{ \left[\frac{H^2 \tanh H}{H - \tanh H} - 3 + \frac{H^2 C_t}{1+C_t} \right] \times 1.3 + 8 \right\}$$

where $H = D_H B \sqrt{\frac{\sigma_c}{\mu}}$ is the Hartmann number

$$\text{and } C_t = \frac{2 t_H \sigma_w}{D_H \sigma_c}$$

In the main text, the blanket thickness has been taken 80 cm. To include the flow passage perpendicular to the B field in the shielding region, the Z used in Δp calculations is 125 cm. To calculate the MHD corner pressure drop at the intersection of the tube and the header the following equation is used [51]:

$$R_1 \equiv \frac{\Delta P_{\text{corner}}}{\Delta p_H} = 0.02 C_t^{1/2} \frac{D_H}{x}$$

Additional pressure drop is due to the space variation of the

field strength. The following equation is used to account for such pressure drop:

$$\Delta P_{\text{fringe}} = K_p \frac{\sigma_c D_H U_H B_{\text{max}}^2}{2} \equiv R_2 \Delta P_H$$

where K_p is a coefficient given in Ref. [52]. For the dimensions of the blankets considered in this study, K_p is less than and taken 0.1.

The total pressure drop is calculated by the following expression, and the safety factor is also determined here:

$$\Delta P_{\text{total}} = F_c \cdot \Delta P_H > \Delta P_H + \Delta P_{\text{corner}} + \Delta P_{\text{fringe}} \equiv F_{cs} \Delta P_s$$

Table A1 summarizes a number of calculated examples of which the parameters are within the range of interest. In these examples, U_H , B_{max} , C_t are constant values. They are:

$$U_H = 0.1 \text{ m/sec}$$

$$B_{\text{max}} = 10 \text{ tesla}$$

$$C_t = 0.034$$

The safety factor used in this study is taken conservatively to accommodate the uncertainties of existing calculational models for pressure drops. When better models are available, the methodology of the systematic analysis can be kept valid by adjusting the safety factor. Better models are needed, for instance, to include effects due to time-varying field and flow in a shape varying pipe in a transverse or

parallel field.

The current leakage through the header walls into the stagnant lithium is not included because a layer of insulation material is assumed to exist on the outer surface of the tube (c.f. Sec. 4.2). This layer is needed because a higher MHD pressure drop is caused by the current leakage. The following is a simplified model for the calculation of such pressure drop if the insulation layer is not used.

Figure A1 shows a rectangular coolant channel of height $2a$, width $2b$, and length L . The magnetic field strength B is normal to the channel and hence is perpendicular to the direction of the coolant velocity U . E is the induced electrical field across the channel from the bottom to the top.

The induced current density is

$$J_Y = \sigma_r (E - UB) \quad (1)$$

Therefore, the current is

$$I = -J_Y 2aL = \sigma_r (2aL)(UB - E) \quad (2)$$

The current will return through the channel wall and the stagnant lithium. The resistance represented by such a path is R .

Therefore,

$$I = \frac{2Eb}{R} = 2Eb \left(\frac{1}{R_w} + \frac{1}{R_{pool}} \right) \quad (3)$$

where R_w is the resistance of the wall and R_{pool} is the resistance of the pool. It is easy to show that $\frac{1}{R_w} = \frac{\sigma_w tL}{2b}$ (4)

Figure A2 shows the model used to calculate R_{pool} . A number

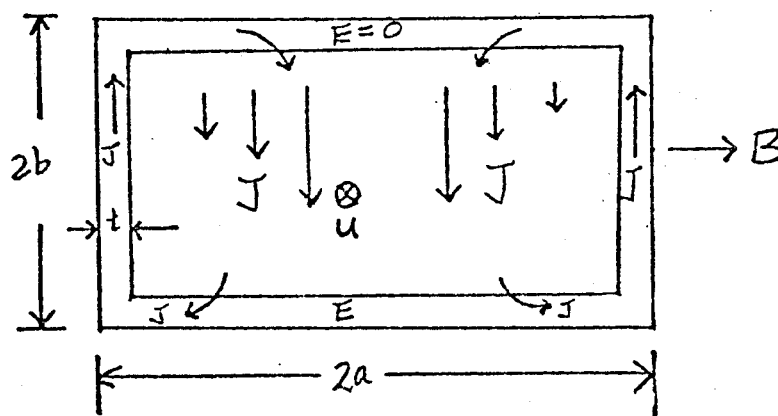


Figure A1. Cross section of a coolant channel with conducting wall

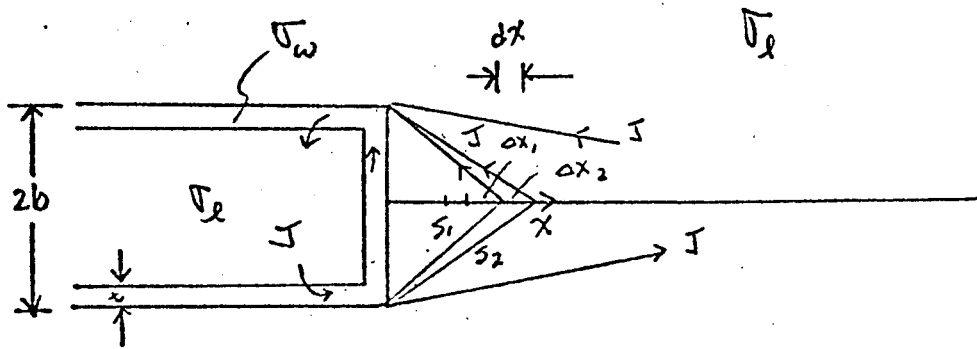


Figure A2. A simple model for the resistance
in the pool

of resistors of conduction length S_i are in parallel.

$$\begin{aligned} \text{Therefore, } \frac{1}{R_{pool}} &= \frac{1}{R_1} + \frac{1}{R_2} + \dots = \frac{\sigma_L}{S_1} \Delta X_1 L + \frac{\sigma_L}{S_2} \Delta X_2 L + \dots \\ &= \sigma_L L \int_0^Y \frac{dX}{S} \end{aligned}$$

$$\therefore \frac{1}{R_{pool}} = \sigma_L L \int_0^L \frac{dX}{2\sqrt{X^2+b^2}} = \frac{\rho}{L} \left(\ln \frac{Y+\sqrt{Y^2+b^2}}{b} \right) \quad (5)$$

Eliminating E from Equations (2) and (3), the expression for I is obtained as follows:

$$I = \frac{\sigma_L (2aL) U B}{1 + \left(\frac{a \sigma_L}{\sigma_w t + b \sigma_L \ln \left(\frac{Y+\sqrt{Y^2+b^2}}{b} \right)} \right)}$$

$$\Delta p = J B L = \frac{I B}{2a} = \frac{L U B^2 \sigma_L}{1 + \left(\frac{\sigma_L a}{\sigma_w t + b \sigma_L \ln \left(\frac{Y+\sqrt{Y^2+b^2}}{b} \right)} \right)}$$

$$\text{for } \sigma_L = 2.2 \times 10^6 \text{ (m}\Omega\text{)}^{-1}$$

$$\sigma_w = 0.95 \times 10^6 \text{ (m}\Omega\text{)}^{-1}$$

$$B = 10 \text{ tesla}$$

$$U = 0.1 \text{ m/sec}$$

$$L = 1.25 \text{ m}$$

$$a = b = 7.45 \text{ cm}$$

$$Y = 4.5 \text{ m}$$

$$\Delta p = 2788 \text{ psi (19.2 Mpa)}$$

If Y is assumed equal to ∞

$$\Delta p = 3988 \text{ psi (27.5 Mpa)}$$

Case Number	$D_H(m)$	$x(m)$	$R_1 \times 10^4$	R_2	F_{cs}
1	0.05	0.5	3.71	0.046	1.046
2	0.07	0.5	5.19	0.064	1.065
3	0.10	0.5	7.42	0.092	1.093
4	0.05	1	1.86	0.046	1.046
5	0.07	1	2.60	0.065	1.065
6	0.15	1	5.57	0.139	1.14
7	0.05	2	0.93	0.046	1.046
8	0.1	2	1.86	0.092	1.092
9	0.15	2	2.78	0.139	1.139
10	0.05	4	0.46	0.046	1.046
11	0.10	4	0.93	0.092	1.092
12	0.15	4	1.39	0.139	1.139
13	0.05	5	0.37	0.046	1.046
14	0.10	5	0.74	0.092	1.092
15	0.15	5	1.11	0.139	1.139
16	0.20	5	1.48	0.185	1.185
17	0.05	6	0.31	0.046	1.046
18	0.10	6	0.62	0.092	1.092
19	0.15	6	0.93	0.139	1.139
20	0.20	6	1.24	0.185	1.185

TABLE AI. The Results of the Examples Calculated for the Various Types of Pressure Drops.

APPENDIX B: METHODS TO CALCULATE THE HOT SPOT TEMPERATURE

The methods to calculate the temperature difference between the tube wall and the maximum temperature, which occurs between the tubes, is illustrated from Fig. B1(a) to Fig. B1(c), where $\Delta T_m = T_m - T_t$ can be written as

$$\Delta T_m = (T_m - T_a) + (T_a - T_t) \quad (B1)$$

The dimension w in Fig. B1(c) is determined by letting the shaded area A equal to area B shown in Fig. B1(d), so that the total heat generated in each area is the same. Then

$$W = b - \frac{\pi}{4} a \quad (B2)$$

The problem shown in Fig. B12(a) is represented by the following equation:

$$k \frac{1}{r} \frac{d}{dr} (r T(r)) + \dot{Q}''' = 0 \quad (B3)$$

With boundary condition:

$$T(D_t/2) = T_t \quad (B4)$$

$$T(a) = T_a \quad (B5)$$

$$k \frac{dT}{dr}(r) = \text{heat generated in the shaded area / unit length entering into the insulated area.}$$

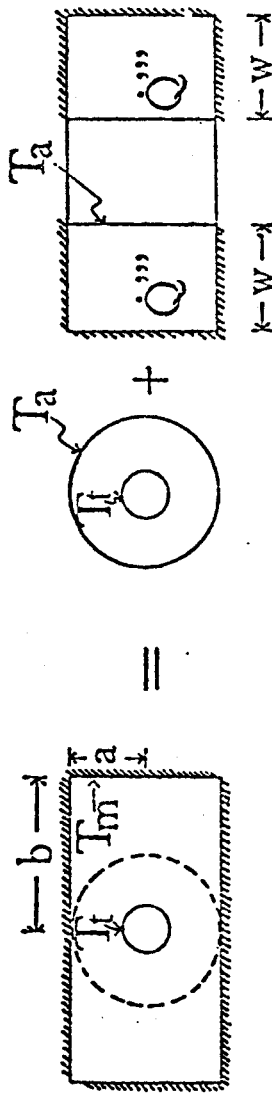


Fig. B1(a)

Fig. B1(b)

Fig. B1(c)

AREA A AREA B



Fig. B1(d)

FIGURE B1. CALCULATION MODELS FOR HOT SPOT TEMPERATURE

$$= \frac{\dot{Q}''' \cdot 2 \cdot (2 a \cdot w)}{2 a \pi} \quad (B6)$$

After the algebra is worked out, $T_a - T_t$ is found to be:

$$T_a - T_t = \frac{\dot{Q}'''}{4K} \left(a^2 - \frac{D_t^2}{4} \right) + a \left[\frac{2(b - \frac{\pi}{4} a) \dot{Q}'''}{\pi K} + \frac{\dot{Q}''' a}{2K} \right] \ln \frac{2a}{D_t} \quad (B7)$$

Similarly, solving the following equation will lead us to the answer to the problem of Fig. B1(b):

$$K \frac{d^2 T(x)}{dx^2} + \dot{Q}''' = 0 \quad (B8)$$

with boundary conditions:

$$T(b-w) = T_a \quad (B9)$$

$$T(b) = T_m \quad (B10)$$

$$\frac{dT}{dx}(b) = 0 \quad (B11)$$

The solution is

$$T_m - T_a = \frac{\dot{Q}'''}{2K} \left(b - \frac{\pi}{4} a \right)^2 \quad (B12)$$

And finally, combining (B7) and (B12), we get,

$$\begin{aligned} \Delta T_m = T_m - T_a &= \frac{\dot{Q}'''}{2K} \left(b - \frac{\pi}{4} a \right)^2 + \frac{\dot{Q}'''}{4K} \left(a^2 - \frac{D_t^2}{4} \right) \\ &+ a \left[\frac{2(b - \frac{\pi a}{4}) \dot{Q}'''}{\pi K} + \frac{\dot{Q}''' a}{2K} \right] \ln \frac{2a}{D_t} \end{aligned} \quad (B13)$$

when $b > a$

or:

$$\Delta T_m = \frac{\dot{Q}'''}{2K} \left(a - \frac{\pi}{4} b \right)^2 + \frac{\dot{Q}'''}{4K} \left(b^2 - \frac{D_t^2}{4} \right) \quad (B14)$$

$$+ b \left[\frac{2(a - \frac{\pi}{4} b) \dot{Q}'''}{\pi K} + \frac{\dot{Q}''' b}{2K} \right] \ln \frac{2b}{D_t}, \quad a > b$$

APPENDIX C: PROGRAM WINDOW

This appendix is a description and listing of the program WINDOW used to generate design windows for the constant \dot{Q} ' configurations. It has been removed for conciseness. The full report may be obtained from the M.I.T. library system as:

J.Chao, 'Thermal-Hydraulic and Neutronic Considerations for Designing a Lithium-Cooled Tokamak Blanket', Ph.D. thesis, M.I.T., Nuclear Engineering, December 1978.

APPENDIX D: DERIVATION OF $U_{H,CRITICAL}$

$U_{H,critical}$ presented in Chapter 2 is derived in this appendix. Equations (6), (7), (8), (9) and (10) in Chapter 2 are rewritten as following:

$$\Delta P_t = 2 F_c \frac{\left(\frac{4}{\pi}\right) Z B_{max}^2 \sigma_w U_H \frac{2 t_H}{D_H}}{1 + \frac{2 t_H}{D_H} \frac{\sigma_w}{\sigma_c}} \quad (C1)$$

$$\frac{D_t}{2t_t} \Delta P_t = \sigma_h \quad (C2)$$

$$\frac{D_H}{t_H} = \frac{D_t}{t_t} \quad (C3)$$

$$\frac{N \Delta P_t (U_H \pi D_H^2)}{\left[\int_0^Z \dot{Q}''' (R) 2\pi (R+R_w) X dR \right]} = C_1 \quad (C4)$$

$$\left[\int_0^Z \dot{Q}''' (R) 2\pi (R+R_w) X dR \right] = N \rho U_H \frac{\pi}{4} D_H^2 C_p \Delta T_c \quad (C5)$$

Substituting Eq. (C2) into Eq. (C1), we obtain the expression for σ_h :

113

$$\sigma_h = \left(\frac{D_t}{2t_t} \right)^2 F_c \left\{ \frac{\frac{4}{\pi} Z B_{\max}^2 \sigma_w U_H \frac{2t_H}{D_H}}{1 + \frac{2t_H \sigma_w}{D_H \sigma_c}} \right\} \quad (C6)$$

Using Eq. (C3), $\frac{t_H}{D_H}$ can be solved by Eq. (C6). Then,

$$\frac{t_H}{D_H} = F_c \left(\frac{4}{\pi} \right) \frac{Z B_{\max}^2 \sigma_c U_H}{\sigma_h} - \frac{\sigma_c}{2\sigma_w} \quad (C7)$$

Substituting Eq. (C5) into Eq. (C4), we obtain the following expression:

$$\Delta P = C_1 \rho C_p \Delta T_c \quad (C8)$$

Using Eqs. (C1) and (C8), we can get the equation to solve for U_H . Then,

$$C_1 \rho C_p \Delta T_c = \frac{\left(\frac{4}{\pi} \right) F_c Z 2 B_{\max}^2 \sigma_w U_H}{\left(1 + \frac{2t_H}{D_H} \frac{\sigma_w}{\sigma_c} \right)} \left(\frac{2t_H}{D_H} \right) \quad (C9)$$

The $\frac{t_H}{D_H}$ term is a function of U_H as shown in Eq. (C7). Therefore, combining Eqs. (C7) and (C9), we can have the expression for U_H .

$$U_H = \frac{C_1 \rho C_p \Delta T_c}{\sigma_c \left(\frac{4}{\pi} \right)^2 F_c Z B_{\max}^2} + \frac{\sigma_h}{2 \sigma_w \left(\frac{4}{\pi} \right) F_c Z B_{\max}^2}$$

The hoop stress should be within a limit (i.e. $\sigma_h \leq \sigma_r$); thus,

$U_H \leq U_{H,critical}$. The $U_{H,critical}$ is:

$$U_{H,critical} = \frac{\pi}{8 F_c Z B_{max}^2} \left(\frac{C_1 \rho C_p \Delta T_c}{\sigma_c} + \frac{\sigma_r}{\sigma_w} \right)$$

Appendix E: Program BEERCANE.1. Description

Program BEERCAN has been developed to generate design for the constant T_{\max} configurations. A typical window is shown in figure 13. The output of the program has been used directly to produce a set of family curves in the figure.

With given values for the blanket thickness and the number of channels, BEERCAN solves the conduction equation in cylindrical coordinates to determine the position of each channel and the peak temperature in the lithium pool. The problem to be solved can be defined as follows:

$$\nabla^2 T(r) + \frac{\dot{Q}}{K} = 0$$

\dot{Q} is in the form:

$$\dot{Q} = KBe^{-vr} \text{ (W/cm}^3\text{)}$$

with boundary conditions:

$$T = r_1, T = T_1$$

$$T = r_2, T = T_2$$

The solution can be found in Ref [53] and is given here:

$$T(r) = T_1 + \frac{A}{bK} + C_1 \ln\left(\frac{r}{r_1}\right) + \frac{B}{b} \left[\int_{r_1}^r \frac{e^{-br}}{r} dr - e^{-br} \right] \quad (E1)$$

where

$$C_1 = T_1 - T_2 + \frac{A}{bK} + \frac{A}{bK} \left[e^{br_1} \int_{r_1}^{r_2} \frac{e^{-br}}{r} dr - e^{-b(r_2 - r_1)} \right].$$

$$\frac{1}{\ln\left(\frac{r_1}{r_2}\right)}, \quad A = KBe^{-br_1}$$

With Eq. (E1) the value of peak temperature and the positions of coolant channels are found by iterative procedures. The procedures are illustrated by the flow chart shown in Fig. E1.

The boundary conditions used in Eq. (E1) provide that the temperatures at the wall channels at equal distance from the inlet header should be equal. Since the heat fluxes at the walls are different from channel to channel the coolant velocities in each channel must be adjusted so that the coolant temperatures rise at the same rate.

More specifically, the coolant velocities must satisfy the following equations:

$$T_{c,i} D_{H,i} \Delta r_i \rho C_p U_i = X D_{H,i} W_i \quad i = 1, \dots, N_{CH} \quad (E2)$$

$$\sum_{i=1}^{N_{CH}} U_i D_{H,i} \Delta r_i = \frac{\pi}{4} D_H^2 U_H \quad (E3)$$

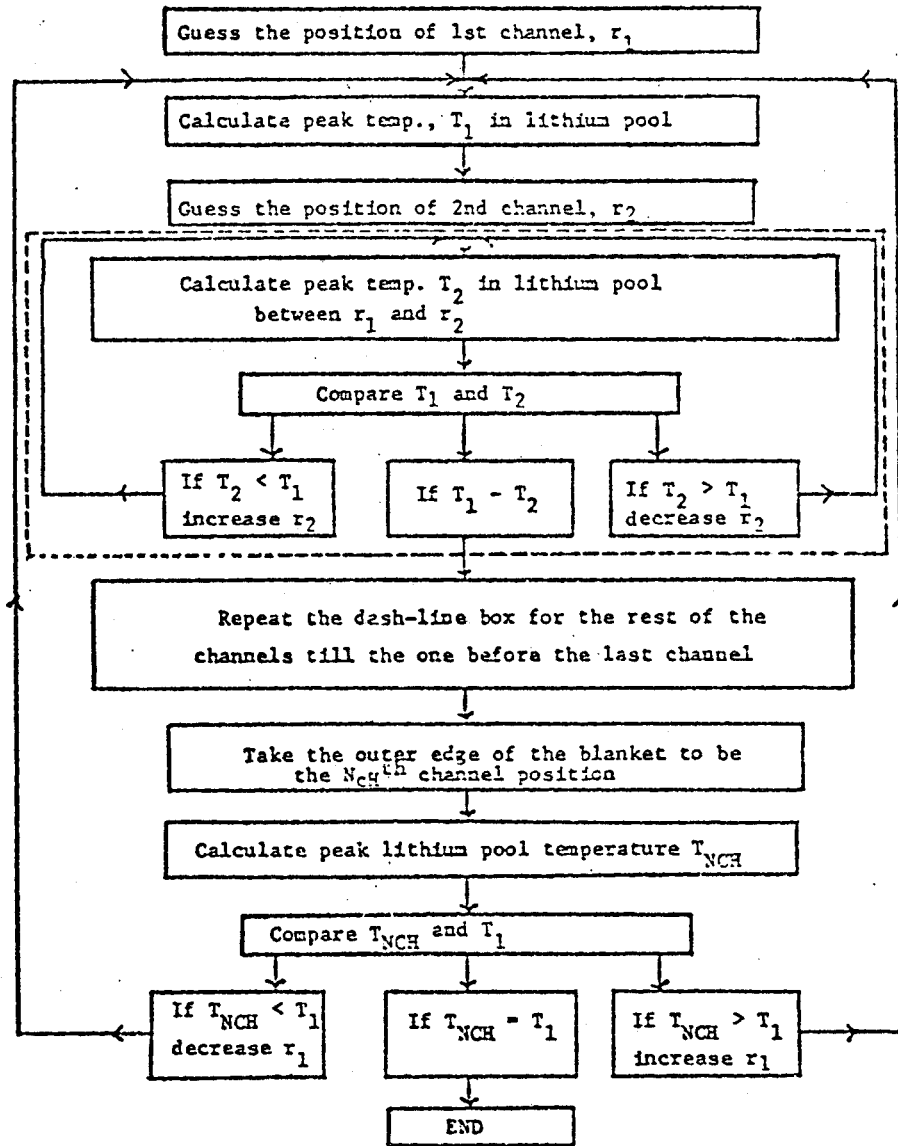


FIGURE E1. FLOW CHART FOLLOWED TO DETERMINE CHANNEL POSITIONS AND PEAK TEMPERATURE IN BEER CAN

With required condition:

$$\frac{\Delta T_{c,1}}{X} = \frac{\Delta T_{c,2}}{X} = \dots = \frac{\Delta T_{c,N_{CH}}}{X} \quad (E4)$$

The above equations are, in fact, used to determine the coolant velocities.

The total number of tubes in the blanket can be solved by Eq. (13) in Chapter 2. The effective channel width Δr_i is assumed a constant for a particular design, and is assigned at channel i such that the cross sectional area of the channel is the same as that covered by tubes.

Thus,

$$\frac{\pi}{4} D_t^2 = D_t \Delta r_i$$

$$\text{or } D_t = \frac{4}{\pi} \Delta r_i$$

The thickness of cooling tubes is determined by specifying a hoop stress within a limit. Thermal stresses can then be calculated with tube thickness and heat fluxes passing through the coolant channels provided by the program WINDOW.

By specifying the temperature rise in the coolant, the constant first wall loading lines are determined as functions of the distance that coolant has travelled. The value of D_H is fixed in this case thus resulting in a constant flow rate.

The $N_{ch} - X$ space depicted in Fig. 12 can be interpreted as an $N_{ch} - q_w$ space, from which the constant peak temperature curve is obtained by the solution to conduction equations.

E.2. Program Listing

The remainder of this appendix contains a listing of the program BEERCAN. It has been removed here for conciseness, but may be obtained from the M.I.T. library system in:

J. Chao, 'Thermal-Hydraulic and Neutronic Considerations for Designing a Lithium-Cooled Tokamak Blanket', Ph.D. thesis, M.I.T., Nuclear Engineering, December 1978.

BRCN0001
 BRCN0002
 BRCN0003
 BRCN0004
 BRCN0005
 BRCN0006
 BRCN0007
 BRCN0008
 BRCN0009
 BRCN0010
 BRCN0011
 BRCN0012
 BRCN0013
 BRCN0014
 BRCN0015
 BRCN0016
 BRCN0017
 BRCN0018
 BRCN0019
 BRCN0020
 BRCN0021
 BRCN0022
 BRCN0023
 BRCN0024
 BRCN0025
 BRCN0026
 BRCN0027
 BRCN0028
 BRCN0029
 BRCN0030
 BRCN0031
 BRCN0032
 BRCN0033
 BRCN0034
 BRCN0035
 BRCN0036

```

CCCCC----- PROGRAM BEER-CAN -----
CCCCC----- DELTA RI ARE FIXED= DRGEN -----
COMMON/SDDT/T1,T2,G,B,N20,F,RW
DIMENSION Q3CH(10),RMID(10),SIZE(10),VELO(10),DTX(10)
DIMENSION DR(10),Q2CH(10,2),RM(10),RE(10,2)
DIMENSION DTC(10),DHI(10),RCA(10)
DIMENSION QTCH(10)
REAL K,NU
NU=6.9
RO=475.0
CP=4200.0

CCCCC
CCCCC----- INPUT BEGINS -----
Z=100.0
T1=500.0
T2=500.0
TCRIT=1000.0
Q=1.0
NCHBGN=5
NCHEND=8
NGAP=1
RW=300.0
A=4.67*Q*RW/300.0
B=0.043
K=0.5
RAF=0.0399
Q2=25*Q
B2=A*EXP(B*RW)/K

CCCCC----- INPUT ENDS -----
CCCCC
N10=10
N20=10
DRGEN=2.0
DH=16.69
PAI=3.1459265
G=A/(K*B**2)

```


BRCN0037
 BRCN0038
 BRCN0039
 BRCN0040
 BRCN0041
 BRCN0042
 BRCN0043
 BRCN0044
 BRCN0045
 BRCN0046
 BRCN0047
 BRCN0048
 BRCN0049
 BRCN0050
 BRCN0051
 BRCN0052
 BRCN0053
 BRCN0054
 BRCN0055
 BRCN0056
 BRCN0057
 BRCN0058
 BRCN0059
 BRCN0060
 BRCN0061
 BRCN0062
 BRCN0063
 BRCN0064
 BRCN0065
 BRCN0066
 BRCN0067
 BRCN0068
 BRCN0069
 BRCN0070
 BRCN0071
 BRCN0072

F=B2/B**2
 NCHM=9
 TSSAL=T2+1.0
 TSMAL=T1+1.0
 RZ=RW+Z
 NCH=NCHBGN
 46 DR(1)=1.5
 DLR1=0.05
 DLR1=0.25
 DLR1=0.5
 DLR1=2.0
 DLR1=1.0
 DY=1.0
 ZGUES=5.0
 ZGUES=2.0
 NHEAD=160
 UH=0.1047
 CCCCC ----- CALCULATION BEGINS -----
 100 FORMAT(' ITERATION',I2,' TMAX=',E13.5)
 101 FORMAT('//',N,RL, RM RR (CM) Q2L Q2R (W/CM2)')
 102 FORMAT(' ',I2,1X,F5.1,2X,F5.1,3X,F5.1,2X,F5.1)
 103 FORMAT('//',BLANKET BECOMES TOO LONG=',F6.1,'CM')
 104 FORMAT(1H1)
 105 FORMAT(' WAIT A MINUTE ----- IT IS SHORT')
 106 FORMAT(' SIZE OF 1ST STAGNATION LI CHANNEL TOO SMALL FOR NCH=',I2)
 107 FORMAT('//',COOLANT CHANNEL R SIZE VELO DT/DX DTC
 5 HEIGHT(MKS) Q3 Q2TOTAL(W/CM2)')
 108 FORMAT(' ',11X,F6.4,3X,F5.4,2X,F6.4,2X,F8.1,4X,F5.2,6X,F5.4,2(2X,E
 611.3))
 109 FORMAT('//',1ST WALL NEUTRON POWER=',F4.1,'MW/M2 TMAX=',F6.1,' C
 7 NO TUBES PER P SLIDE=',F8.1)
 110 FORMAT('//',MAX POWER LEVEL=',F4.1,'MW/M2')
 111 FORMAT('//',A1=',F8.5,' A2=',F8.5,' ALPHA=A1+A2/X X IN METER')
 190 FORMAT(' DT/DR=',E13.5,' R=',E13.5,' R1=',E13.5,' R2=
 2,E13.5)
 197 FORMAT(' TEMP=',E13.5,' AT R=',E13.5,' R1=',E13.5,' R2=',E13

BRCN0073
 BRCN0074
 BRCN0075
 BRCN0076
 BRCN0077
 BRCN0078
 BRCN0079
 BRCN0080
 BRCN0081
 BRCN0082
 BRCN0083
 BRCN0084
 BRCN0085
 BRCN0086
 BRCN0087
 BRCN0088
 BRCN0089
 BRCN0090
 BRCN0091
 BRCN0092
 BRCN0093
 BRCN0094
 BRCN0095
 BRCN0096
 BRCN0097
 BRCN0098
 BRCN0099
 BRCN0100
 BRCN0101
 BRCN0102
 BRCN0103
 BRCN0104
 BRCN0105
 BRCN0106
 BRCN0107
 BRCN0108

```

4.5)
120 FORMAT(/, ' IF YOU THINK ITS TOO SHORT RUN THE PROGRAM AGAIN WITH L
      7ONGER 1ST LI CHANNEL SIZE')
121 FORMAT(/, ' NO OF COOLANT CHANNELS IS=', I2)
122 FORMAT(/, ' THERMAL STRESS PSI/COOLANT CHANNEL=', 9(2X,F7.1))
      DO 45 LP=1,NCH
      DR(LP)=DRGEN
45 CONTINUE
      CPY=(Z-ZGUES)/(NCH-1)
      IF(NCH.LE.2) GO TO 28
      GO TO 29
28 CPY=Z-2.0*DR(1)
29 NCOUT=1
21 N=1
      R1=DR(1)+RW
      GO TO 24
23 CPY=CPY-DLR1*0.5
      N=1
      R1=DR(1)+RW
24 R2=R1+CPY
      IF(R2.LE.R1) GO TO 25
      R=R1
      CCCCC----- CHANNEL 1 -----
      CALL DDT(R1,R2,R,DTDR)
      Q2CH(N,1)=DTDR*K
      Q2CH(N,1)=ABS(Q2CH(N,1))
      R=R2
      CALL DDT(R1,R2,R,DTDR)
      Q2CH(N,2)=DTDR*K
      Q2CH(N,2)=ABS(Q2CH(N,2))
      CCCCC----- Q2 ON BOTH SIDE CF REGION 1 CALCULATED ----
      Q2CHW=Q2
      R=R1+DLR1
11 CALL DDT(R1,R2,R,DTDR)
      IF(DTDR.LE.0) GO TO 10
      R=R+DLR1

```

```

GO TO 11
10 RM(N)=R
CCCCC----- R AT TMAX FOUND -----
      CALL FUSE(R1,RM(N),TR,R2)
      TMAX=TR
      IF(TMAX.LE.TSMAL) GO TO 25
      IF(TMAX.LE.TSSAL) GO TO 25
CCCCC----- TMAX1 CALCULATED -----
      RE(N,1)=R1
      RE(N,2)=R2
      WRITE(6,100) NCOU,TMAX
      WRITE(6,102) N,RE(N,1),RM(N),RE(N,2),Q2CH(N,1),Q2CH(N,2)
      IF(NCH.LE.2) GO TO 18
      N=2
19 NM=N-1
      RE(N,1)=RE(NM,2)+DR(N)
      R1=RE(N,1)
      R2=RE(N,1)+CPY*1.02
14 R=R1+DLR1
13 CALL DDT(R1,R2,R,DTDR)
      IF(DTDR.LE.0) GO TO 12
      R=R+DLR1
CCCCC----- CALCULATE NEXT CHANNEL TMAX AND ITS R -----
      GO TO 13
12 CALL FUSE(R1,R,TR,R2)
      IF(TR.GE.TMAX) GO TO 15
      R2=R2+DLR1
      IF(R2.GT.RZ) GO TO 23
      GO TO 14
15 WRITE(6,197) TR,R,R1,R2
      RM(N)=R
CCCCC----- TMAX AND ITS R FOUND -----
      RE(N,2)=R2
      CALL DDT(RE(N,1),RE(N,2),RE(N,1),DTDR)
      Q2CH(N,1)=K*DTDR
      Q2CH(N,1)=ABS(Q2CH(N,1))

```

BRCN0109
 BRCN0110
 BRCN0111
 BRCN0112
 BRCN0113
 BRCN0114
 BRCN0115
 BRCN0116
 BRCN0117
 BRCN0118
 BRCN0119
 BRCN0120
 BRCN0121
 BRCN0122
 BRCN0123
 BRCN0124
 BRCN0125
 BRCN0126
 BRCN0127
 BRCN0128
 BRCN0129
 BRCN0130
 BRCN0131
 BRCN0132
 BRCN0133
 BRCN0134
 BRCN0135
 BRCN0136
 BRCN0137
 BRCN0138
 BRCN0139
 BRCN0140
 BRCN0141
 BRCN0142
 BRCN0143
 BRCN0144

```

BRCN0145
BRCN0146
BRCN0147
BRCN0148
BRCN0149
BRCN0150
BRCN0151
BRCN0152
BRCN0153
BRCN0154
BRCN0155
BRCN0156
BRCN0157
BRCN0158
BRCN0159
BRCN0160
BRCN0161
BRCN0162
BRCN0163
BRCN0164
BRCN0165
BRCN0166
BRCN0167
BRCN0168
BRCN0169
BRCN0170
BRCN0171
BRCN0172
BRCN0173
BRCN0174
BRCN0175
BRCN0176
BRCN0177
BRCN0178
BRCN0179
BRCN0180

CALL DDT(RE(N,1),RE(N,2),RE(N,2),DTDR)
Q2CH(N,2)=K*DTDR
Q2CH(N,2)=ABS(Q2CH(N,2))
CCCCC----- Q2 ON BOTH SIDE OF REGION CALCULATED -----
WRITE(6,102) N,RE(N,1),RM(N),RE(N,2),Q2CH(N,1),Q2CH(N,2)
CCCCC----- GO FOR NEXT CHANNEL-- FOR TMAX AND R -----
NY=NCH-1
IF(N.GE.NY) GO TO 18
N=N+1
CCCCC----- NEXT CHANNEL SIZE ALLOVER AGAIN-----
GO TO 19
CCCCC----- LAST CHANNEL SIZE CALCULATED-----
18 RFNL=DR(NCH)+RE(N,2)
WRITE(6,103) RFNL
IF(RFNL.LE.RZ) GO TO 20
CPY=CPY-DLR1*0.2
NCOUT=NCOUT+1
GO TO 21
20 WRITE(6,105)
WRITE(6,120)
WRITE(6,104)
WRITE(6,101)
NK=NCH-1
DO 22 M=1,NK
WRITE(6,102) M,RE(M,1),RM(M),RE(M,2),Q2CH(M,1),Q2CH(M,2)
22 CONTINUE
CCCCC----- CALCULATE Q3 IN EACH COOLANT CHANNEL -----
CCCCC----- CALCULATE COOLANT CHANNEL MID POSITION-----
IF(NCH.LE.2) GO TO 27
DO 31 NT3=2,NK
NTJ=NT3-1
R1=RE(NTJ,2)
R2=RE(NT3,1)
RMID(NT3)=0.5*(R1+R2)
SIZE(NT3)=R2-R1
CALL COOHET(R1,R2,K,B2,YCD)

```

```

BRCN0181
BRCN0182
BRCN0183
BRCN0184
BRCN0185
BRCN0186
BRCN0187
BRCN0188
BRCN0189
BRCN0190
BRCN0191
BRCN0192
BRCN0193
BRCN0194
BRCN0195
BRCN0196
BRCN0197
BRCN0198
BRCN0199
BRCN0200
BRCN0201
BRCN0202
BRCN0203
BRCN0204
BRCN0205
BRCN0206
BRCN0207
BRCN0208
BRCN0209
BRCN0210
BRCN0211
BRCN0212
BRCN0213
BRCN0214
BRCN0215
BRCN0216

Q3CH(NT3)=YCD
31 CONTINUE
R1=RW
R2=RE(1,1)
RMID(1)=0.5*(R1+R2)
SIZE(1)=R2-R1
CALL COHET(R1,R2,K,B2,YCD)
Q3CH(1)=YCD
R1=RE(NK,2)
R2=RZ
CALL COHET(R1,R2,K,B2,YCD)
Q3CH(NCH)=YCD
RMID(NCH)=0.5*(R1+R2)
SIZE(NCH)=R2-R1
GO TO 30

27 R1=RW
R2=RE(1,1)
SIZE(1)=R2-R1
RMID(1)=(R1+R2)*0.5
CALL COHET(R1,R2,K,B2,YCD)
Q3CH(1)=YCD
R1=RE(1,2)
R2=RZ
SIZE(2)=R2-R1
RMID(2)=(R1+R2)*0.5
CALL COHET(R1,R2,K,B2,YCD)
Q3CH(2)=YCD

CCCC----- Q3 AND MID POSITION OF COOLANT CHANNELS FOUND -----
30 P1=RW*2.0*PAI/NHEAD
P2=(RZ+25.0)*2.0*PAI/NHEAD
CCCC----- CALCULATE HEIGHT OF COOLANT CHANNELS -----
DO 32 JS=1,NCH
DHI(JS)=(RMID(JS)-RW)*(P2-P1)/(Z+25.0)+P1
32 CONTINUE
CCCC----- CALCULATE TOTAL HEAT IN THE COOLANT -----
IF(NCH.LE.2) GO TO 34

```

```

BRCN0217
BRCN0218
BRCN0219
BRCN0220
BRCN0221
BRCN0222
BRCN0223
BRCN0224
BRCN0225
BRCN0226
BRCN0227
BRCN0228
BRCN0229
BRCN0230
BRCN0231
BRCN0232
BRCN0233
BRCN0234
BRCN0235
BRCN0236
BRCN0237
BRCN0238
BRCN0239
BRCN0240
BRCN0241
BRCN0242
BRCN0243
BRCN0244
BRCN0245
BRCN0246
BRCN0247
BRCN0248
BRCN0249
BRCN0250
BRCN0251
BRCN0252

DO 33 IA=2,NK
IA1=IA-1
QTCH(IA) = (Q2CH(IA1,2)*RE(IA1,2)+Q2CH(IA,1)*RE(IA,1))
QTCH(IA) = QTCH(IA) / (RE(IA1,2)+RE(IA,1))
QTCH(IA) = Q3CH(IA) + QTCH(IA)
33 CONTINUE
QTCH(1) = (Q2CH*RW+Q2CH(1,1)*RE(1,1))/(RW+RE(1,1))
QTCH(1) = QTCH(1) + Q3CH(1)
QTCH(NCH) = Q3CH(NCH) + (Q2CH(NK,2)*RE(NK,2))/(RZ+RE(1,1))
GO TO 35
34 Q2CH(1) = Q3CH(1) + (Q2CH*RW+Q2CH(1,1)*RE(1,1))/(RW+RE(1,1))
Q2CH(2) = Q3CH(2) + Q2CH(1,2)*RE(1,2)/(RZ+RE(1,2))
35 SUM=0.0
CCCC----- CALCULATE COOLANT VELOCITY -----
DO 36 NB=1,NCH
SUM=SUM+DHI(NB)*QTCH(NB)
36 CONTINUE
U=PAI*0.25*P2*P2*UH/SUM
DO 37 NC=1,NCH
VELO(NC) = QTCH(NC) * U / SIZE(NC)
37 CONTINUE
DO 43 IR=1,NCH
RMID(IR) = RMID(IR) * 0.01
SIZE(IR) = SIZE(IR) * 0.01
DHI(IR) = DHI(IR) * 0.01
43 CONTINUE
WRITE(6,107)
CCCC----- CALCULATE DT/DX -----
FONPY=10000.0*Q/(RO*CP)
FONZY=4.0/(K*NU*PAI**2.0)
DO 39 ID=1,NCH
DTX(ID) = FONPY*QTCH(ID) / (VELO(ID)*SIZE(ID))
DTX(ID) = DTX(ID)*2.0
39 CONTINUE
CCCC----- CALCULATE DT FILM -----
DO 40 IE=1,NCH

```

```

Q TCH(IE) =QTCH(IE) -Q3CH(IE)
DTC(IE) =FONZY*QTCH(IE) *SIZE(IE) *100.0
40 CONTINUE
DO 38 ND=1,NCH
WRITE(6,108) RMID(ND),SIZE(ND),VELO(ND),DTX(ND),DTC(ND),DHI(ND),Q3
7CH(ND),QTCH(ND)
38 CONTINUE
DO 41 IH=1,NCH
RCA(IH) =RMID(IH)
RMID(IH) =RMID(IH) *PAI**2.0*0.5/SIZE(IH)
41 CONTINUE
SUMM=0.0
DO 42 IP=1,NCH
SUMM=SUMM+RMID(IP)
42 CONTINUE
WRITE(6,109) Q,TMAX,SUMM
QCRIT=Q*(TCRIT-T1)/(TMAX-T1)
WRITE(6,110) QCRIT
CCCC----- CALCULATE STRUCTURE PERCENTAGE -----
YP=(P2-P1)/(Z+25.0)
A2=2.0*NHEAD*RAF*(Z**3.0*YP**2.0/3.0+P1*YP*Z**2.0+P1**2.0*Z)
A2=A2/(PAI*(RZ**2.0-RW**2.0))
A2=A2*0.01
SUM1=0.0
DO 44 NP=1,NCH
SUM1=SUM1+RCA(NP) *SIZE(NP)
44 CONTINUE
A1=SUM1*8.0*RAF/(PAI*(RZ**2.0-RW**2.0))
A1=A1*PAI*10000.0
WRITE(6,111) A1,A2
WRITE(6,121) NCH
DO 48 IQ=1,NCH
SIZE(IQ) =145000.0*SIZE(IQ) *RAF*QTCH(IQ)
48 CONTINUE
WRITE(6,122) (SIZE(IQ),IQ=1,NCH)
GO TO 26

```

```

BRCN0253
BRCN0254
BRCN0255
BRCN0256
BRCN0257
BRCN0258
BRCN0259
BRCN0260
BRCN0261
BRCN0262
BRCN0263
BRCN0264
BRCN0265
BRCN0266
BRCN0267
BRCN0268
BRCN0269
BRCN0270
BRCN0271
BRCN0272
BRCN0273
BRCN0274
BRCN0275
BRCN0276
BRCN0277
BRCN0278
BRCN0279
BRCN0280
BRCN0281
BRCN0282
BRCN0283
BRCN0284
BRCN0285
BRCN0286
BRCN0287
BRCN0288

```

```

25 WRITE(6,106) NCH
26 IF(NCH.LE.NCHEND) GO TO 47
   NCH=NCH-NGAP
   GO TO 46
47 STOP
   END
   SUBROUTINE GFD(X1,Y1,EPY)
   COMMON/SDDT/T1,T2,G,B,N20,F,RW
192 FORMAT(' SUBROUTINE GFD GIVES INTEGRAL=',E13.5,' X1=',E13.5,'
   Y1=',E13.5)
   J=1
   FN20=FLOAT(N20)
   DF=(Y1-X1)/FN20
   S=X1+DF*0.5
   EPY=0.0
1001 EPY=EPY+DF*EXP(-B*S)/S
   IF(J.GE.N20) GO TO 1000
   J=J+1
   S=S+DF
   GO TO 1001
1000 RETURN
   END
   SUBROUTINE CON1(R1,R2,C1)
   COMMON/SDDT/T1,T2,G,B,N20,F,RW
   Y1=R2
   X1=R1
   CALL GFD(X1,Y1,EPY)
194 FORMAT(' SUBROUTINE INTEGRAL JUST USED')
   C1=EPY*EXP(B*R1)
   C1=C1+1-EXP(-B*(R2-R1))
   C1=C1*G*EXP((RW-R1)*B*1.0)+T1-T2
   C1=C1/ALOG(R1/R2)
191 FORMAT(' SUBROUTINE CON1 GIVES C1=',E13.5,' R1=',E13.5,' R2=',
   3E13.5)
   RETURN
   END

```

```

BRCN0289
BRCN0290
BRCN0291
BRCN0292
BRCN0293
BRCN0294
BRCN0295
BRCN0296
BRCN0297
BRCN0298
BRCN0299
BRCN0300
BRCN0301
BRCN0302
BRCN0303
BRCN0304
BRCN0305
BRCN0306
BRCN0307
BRCN0308
BRCN0309
BRCN0310
BRCN0311
BRCN0312
BRCN0313
BRCN0314
BRCN0315
BRCN0316
BRCN0317
BRCN0318
BRCN0319
BRCN0320
BRCN0321
BRCN0322
BRCN0323
BRCN0324

```


BRCN0325
 BRCN0326
 BRCN0327
 BRCN0328
 BRCN0329
 BRCN0330
 BRCN0331
 BRCN0332
 BRCN0333
 BRCN0334
 BRCN0335
 BRCN0336
 BRCN0337
 BRCN0338
 BRCN0339
 BRCN0340
 BRCN0341
 BRCN0342
 BRCN0343
 BRCN0344
 BRCN0345
 BRCN0346
 BRCN0347
 BRCN0348
 BRCN0349
 BRCN0350
 BRCN0351
 BRCN0352
 BRCN0353
 BRCN0354
 BRCN0355
 BRCN0356
 BRCN0357
 BRCN0358
 BRCN0359
 BRCN0360

```

SUBROUTINE DDT(R1,R2,R,DTDR)
COMMON/SDDT/T1,T2,G,B,N20,F,RW
CALL CON1(R1,R2,C1)
193 FORMAT(' SUBROUTINE C1 JUST USED')
DTDR=EXP(-B*R)*(B+1/R)
DTDR=F*DTDR
DTDR=DTDR+C1/R
RETURN
END
SUBROUTINE FUSE(R1,R,TR,R2)
COMMON/SDDT/T1,T2,G,B,N20,F,RW
195 FORMAT(' SUBROUTINE INTEGRAL JUST USED')
196 FORMAT(' SUBROUTINE C1 JUST USED')
X1=R1
Y1=R
CALL GFD(X1,Y1,EPY)
EPY=EPY-EXP(-B*R)
EPY=EPY+EXP(-B*R1)
TR=EPY*F+T1
CALL CON1(R1,R2,C1)
TR=TR+C1*ALOG(R/R1)
RETURN
END
SUBROUTINE COHET(R1,R2,K,B2,YCD)
COMMON/SDDT/T1,T2,G,B,N20,F,RW
REAL K,NU
FN20=FLOAT(N20)
DY=(R2-R1)/FN20
S1=R1
S1=S1+DY*0.5
L=1
RDDT=R1+R2
COHOT=0.0
1002 COHOT=COHOT+EXP(-B*(S1-RW))*S1*DY
IF(L.GE.N20) GC TO 1003
L=L+1

```

BRCN0361
BRCN0362
BRCN0363
BRCN0364
BRCN0365
BRCN0366
BRCN0367
BRCN0368
BRCN0369
BRCN0370

```
S1=S1+DY
GO TO 1002
1003 YCD=COHOT*G*K*B**2.0*EXP((RW-R1)*B)/RDDT
      WRITE(6,198) G,B,K
      WRITE(6,199) R1,R2,RDDT,COHOT,YCD
198 FORMAT(/,' SUBRNT COHET GIVES G=',E11.3,' B=',E11.3,' K=',E11.3)
199 FORMAT(' R1 R2 RDDT COHOT YCD ARE ',5(2X,E11.3))
      RETURN
      END
//G.SYSIN DD *
```

APPENDIX F: PROGRAM NEBULAF1. Heat generation calculation

The program NEBULA has been developed to calculate the volumetric heat generation rate and radiation damage rates.

For multigroup calculation, the volumetric heat generation is expressed as the following:

$$Q_{\alpha}^n = \sum_{\beta=1}^{100} \phi_{\alpha\beta} \sum_{\gamma} n_{\alpha\gamma} K_{\beta\gamma}$$

$$Q_{\alpha}^G = \sum_{\beta=101}^{121} \phi_{\alpha\beta} \sum_{\gamma} n_{\alpha\gamma} B_{\beta\gamma}$$

$$Q_{\alpha}^T = Q_{\alpha}^G + Q_{\alpha}^n$$

where:

$$Q_{\alpha}^G = \text{volumetric heat generation due to gamma heating at position } \alpha \left(\frac{\text{ev}}{\text{cm}^3 \cdot \text{sec}} \right)$$

$$Q_{\alpha}^n = \text{volumetric heat generation due to the neutron heating at position } \alpha \left(\frac{\text{ev}}{\text{cm}^3 \cdot \text{sec}} \right)$$

$$Q_{\alpha}^T = \text{total volumetric heat generation at position } \alpha \left(\frac{\text{ev}}{\text{cm}^3 \cdot \text{sec}} \right)$$

$\phi_{\alpha\beta}$ = neutron or gamma flux of group β at position α $(\text{cm}^2\text{sec})^{-1}$

$n_{\alpha\gamma}$ = number density of material γ at position α $(\text{atom}/\text{cm}^3 \times 10^{-24})$

$K_{\beta\gamma}$ = kerma factor of material γ , group β (ev-barn)

The difficulties of using ANISN to calculate the Q 's which necessitate developing of NEBULA are the following:

a) ANISN only calculates the quantity

$$D_{\alpha\gamma} \equiv \sum_{\beta=1}^{121} \phi_{\alpha\beta} n_{\alpha\beta} K_{\beta\gamma}$$

To get Q_{α}^T , additional calculation is needed. Even only for $D_{\alpha\gamma}$, more artificial ANISN materials^(*) need to be added in the mixing table^(*) of input and that causes more complication for inputting ANISN, which has already been a complex task.

b) When ANISN calculates $D_{\alpha\gamma}$, the summation is taken from $\beta = 1$ to $\beta = 121$.

Therefore, information on Q_{α}^n or Q_{α}^G each is lost.

c) Kerma factor's from DLC-37D used to calculate Q_{α} or $Q_{\alpha\gamma}$ are of 121 groups. Thus, there are 121 numbers of Kerma values for each material. In DLC-37D, Kerma factors of 26 materials are given in a 121 x 124 matrix, filled with numbers from first row to twenty-sixth row and the rest filled with zero's. In an ANISN run this Kerma matrix is treated

*See Ref. [3] for the definition

as one of the ANISN materials and is mixed with other materials in the mixing table.

When ANISN runs in group collapsing mode and generates few group cross sections, the scattering cross sections filled in the fourth row and below are shrunk differently from absorption, fission and total cross sections, which occupy the first three rows in a matrix. This shrinking procedure of scattering cross sections does not apply to the kermas. The few group kermas shrunk by ANISN are, thus, incorrect except those in the first three rows. Therefore, ANISN is not capable of calculating Q_{α} or $D_{\alpha\gamma}$ for a few group runs.

NEBULA is then coded to calculate Q_{α}^T , Q_{α}^n , Q_{α}^G individually, with neutron and gamma fluxes supplied by ANISN punched output and Kerma's obtained from DLC-37D.

The capability of calculating heat generation with a few group structures is another feature of NEBULA. The few group fluxes (of 26 groups) are expanded into 121 groups weighted by 121 group fluxes, from any appropriate 121 group ANISN run, to match the kermas of 121 groups.

F2. Radiation Damage Rates

NEBULA can also be used to calculate radiation damage rates in terms of displacements per atom, hydrogen production rate, and helium production rate. In this case, the Kerma's are replaced by multigroup displacement cross sections or gas production cross sections generated by RECOIL.

The radiation damage rate is then:

$$R_{\alpha}^i = \sum_{\beta=1}^{100} \phi_{\alpha\beta} \sum_{\gamma} n_{\alpha\gamma} \sigma_{\beta\gamma}^i$$

where:

R_{α}^i = radiation damage rate of the i^{th} kind

$\sigma_{\beta\gamma}^i$ = cross sections of material γ , group β

$i = 1, 2$ or 3 stands for displacements per atom, hydrogen production rate, or helium production rate, respectively.

F.3. Program Listing

The remainder of this appendix contains a listing of the program NEBULA. It has been removed here for conciseness, but may be obtained from the M.I.T. library system in:

J. Chao, 'Thermal-Hydraulic and Neutronic Considerations for Designing a Lithium-Cooled Tokamak Blanket', Ph.D. thesis, M.I.T., Nuclear Engineering, December 1978.